



A coupled-mode model for the scattering of water waves by shearing currents in variable bathymetry

Journal:	<i>Journal of Fluid Mechanics</i>
Manuscript ID:	draft
mss type:	Standard
Date Submitted by the Author:	n/a
Complete List of Authors:	Belibassakis, K.A.; Dept of Naval Architecture Marine Engineering, National Technical University of Athens; Dept of Naval Architecture Marine Engineering, National Technical University of Athens
Keyword:	Waves/Free-surface Flows, Topographic effects < Geophysical and Geological Flows, Variational methods < Mathematical Foundations

A coupled-mode model for the scattering of water waves by shearing currents in variable bathymetry

K. A. BELIBASSAKIS

School of Naval Architecture and Marine Engineering
National Technical University of Athens
Heron Polytechniou 9, Zografos 15773, Athens, Greece
Tel: (+30) 2107721138, Fax: (+30) 2107721397
E-mail: kbel@fluid.mech.ntua.gr

Abstract

A coupled-mode model is presented for wave-current-seabed interaction, with application to the problem of wave scattering by ambient shearing currents in variable bathymetry regions. We consider obliquely incident waves on a horizontally non-homogeneous current in a variable-depth strip, which is characterized by straight and parallel bottom contours. The flow associated with the current is assumed to be directed along the bottom contours and it is considered to be steady and known. In a finite subregion containing the bottom irregularity, we assume that the current has an arbitrary horizontal structure. Outside this region, the current is assumed to be uniform (or zero). Based on a variational principle, in conjunction with a rapidly-convergent local-mode series expansion of the wave pressure field in a finite subregion containing the current variation and the bottom irregularity, a new coupled-mode system of equations is obtained, governing the scattering of waves in the presence of variable bathymetry and longshore shearing currents. By keeping only the propagating mode in the local-mode series, a new one-equation model is derived, having the property to reduce to modified mild-slope equation (Massel 1993, Chamberlain & Porter 1995), when the current is zero, and to the enhanced mild-shear equation (McKee 1996), when the bottom is flat. An important aspect of the present model is that it can be further elaborated to treat shearing currents with general, depth-dependent vertical structure, and to include the effects of weak nonlinearity.

Keywords: Waves/Free-surface flows, topographic effects, variational methods

1. Introduction

Except of depth variations, the presence of currents significantly influences the propagation of waves in the nearshore and coastal environment. The detailed knowledge of the wave characteristics in the presence of ambient currents and bottom variations is important for various applications, as for example, in coastal and harbour engineering problems, in the study of oil slick dispersion and pollutant transport in nearshore and coastal waters, as well as for sediment transport and coastal erosion studies. Extensive reviews on the subject of wave-current interaction in the sea and in the nearshore region have been presented by Peregrine (1976), Jonsson (1990), Thomas & Klopman (1997).

Non-homogeneous shearing currents, following or opposing wavetrains, produce significant changes on the wave characteristics, especially in the region where there is a rapid change of current strength. Thus, large amplitude waves may appear as a result of interaction of obliquely propagating waves with adverse currents; see, e.g., Mei (1983, Chap.3.7), Jonsson (1990, Sec.1B). Wave amplification could be further enhanced by inshore effects due to sloping seabeds, and has sometimes been reported to be connected with the appearance of “giant waves” in coastal waters; see, e.g., Faulkner (2000), Dysthe (2000).

Wave-current interaction models over slowly varying bottom topography have been developed and studied by various authors. Under the assumption of irrotational wave motion, Kirby (1984) derived a phase-resolving one-equation model, generalizing the mild-slope equation (Eckart 1952, Berkhoff 1972) in regions with slowly varying depth and ambient currents, and modifying previous derivations by Booij (1981) and Liu (1983); see also Liu (1990). The latter model in its elliptic time-harmonic form has been exploited, in conjunction with numerical (finite-element, finite difference etc) solvers, to numerous wave-current-seabed interaction applications; see, e.g., Chen *et al* (2005) and the references cited there.

On the other hand, if the wave flow is assumed to be weakly rotational, as happens to be the case when waves are scattered by shearing currents characterised by stronger horizontal gradients, McKee (1987) derived another one-equation model, called the mild-shear equation, based on the linearised Euler equations (see, e.g., Mei 1983, Chap. 3.6). Still however, the validity of the mild-shear equation is based on the assumption of slow

current and depth variations compared to the typical wavelength. In the case of flat bottom, the mild-shear model has been further enhanced by McKee (1996) by including an extra term and obtaining the so called enhanced mild-shear equation. The latter model is applicable to cases where the shearing current is varying on the scale of the wavelength. In the above works by McKee (1987, 1996) the current is considered to be flowing along one horizontal direction while the bottom topography varies in the other horizontal direction. Thus, the mild-shear model is more appropriate for problems of wave scattering by slowly varying depth and longshore-type ambient shearing currents.

In both the above approaches (mild-slope model, mild-shear model) the effects of evanescent modes, describing higher-order localised effects due to bottom and current variations, have been ignored. Except of the above models based on irrotational and weakly rotational assumption concerning the wave motion, another class of wave-current-seabed interaction models have been developed, applicable to cases where the lateral length scale on which the medium (bottom topography and current) is changing is much smaller than the typical wavelength. In this case, the problem has been modelled by means of step discontinuities and vertical vortex sheets, separating subregions of essentially potential flow, in conjunction with appropriate matching conditions ensuring continuity of pressure and normal flow following the vortex sheet. In this context, generalising the work by Evans (1975) for the transmission of deep-water waves across a vortex sheet, Smith (1983, 1987) presented models treating the problem of waves crossing uniform current jets in constant finite depth and crossing a step with horizontal shear, respectively. Also, Kirby *et al* (1987) studied the propagation of obliquely incident waves over a trench with uniform current flowing along it. In the latter models complete representations of the wave potentials in the various subregions have been used, containing both the propagating and the evanescent modes, which are necessary in order to satisfy the matching/boundary conditions at the vertical interfaces (vortex sheets and depth discontinuities). Finally, the approach by Smith (1987) and Kirby *et al* (1987) has been further exploited by McKee (2003) to study scattering of waves by shearing currents of general horizontal structure in water of constant depth. In the latter work the current is modelled by a series of vertical vortex sheets separating subregions of constant current velocity, and the solution is again obtained by using complete representations of the wave potential in each subregion and matching conditions at the vertical interfaces. Also, in McKee (2003) systematic comparisons have been presented between the predictions by

the mild-shear equation(s) and the piecewise constant current velocity approximation, which is considered as more exact, showing that the accuracy of the enhanced mild-shear equation is generally better than the original mild-shear equation. Furthermore, it is shown in the same work that in cases of waves interacting with strong adverse shearing currents, as well as in cases where the current variation length is much smaller than the wavelength, the accuracy of the simplified mild-shear models is lost.

In the present work, a continuous coupled-mode model is developed for the scattering of water waves by horizontally shearing currents in variable bathymetry regions, without any asymptotic assumption or restriction concerning the smallness of the bottom and current variation length with respect to the local wavelength. We consider obliquely incident harmonic waves on a horizontally non-homogeneous current in a variable-depth strip, characterized by straight and parallel bottom contours; see Fig.1. For simplicity, the flow associated with the current is assumed to be parallel to the bottom contours and it is considered to be uniform in depth and known. In a finite subregion containing the bottom irregularity we assume an arbitrary horizontal current structure. Outside this region, the current is assumed to be uniform (or zero). Under the smallness assumption concerning the steepness of the waves, the problem is governed by the linearised Euler equations, the free-surface and the bottom no-entrance boundary conditions, as described in Sec. 2.

The present coupled-mode system of equations on the horizontal plane is obtained by an appropriate variational principle, described in Sec. 3 and in the Appendix, in conjunction with a rapidly-convergent local-mode series expansion of the wave pressure field in the finite subregion containing the current variation and the bottom irregularity, discussed in Sec. 4. The local-mode series contains, except of the propagating and evanescent modes, an additional term, called the sloping-bottom mode, first introduced by Athanassoulis & Belibassakis (1999) for the propagation of water waves in variable bathymetry regions. The sloping-bottom mode enables the consistent satisfaction of the Neumann boundary condition on the non-horizontal parts of the bottom, and substantially accelerates the rate of convergence of the local-mode series. Thus, for all practical applications, a small number of modes (of the order of 4 – 5, including the propagating mode, the sloping-bottom mode and the first few evanescent modes) is found to be enough for an accurate numerical solution. Moreover, by keeping only the propagating mode in the local-mode

series, a new one-equation model has been derived and discussed in Sec 4.2, called the *mild slope and shear equation*. This new model approximately describes the combined scattering effects due to shearing current and bottom irregularities, and consistently generalises both the modified mild-slope equation (Massel 1993, Chamberlain & Porter 1995) and the enhanced mild-shear equation (McKee 1996), having the property to exactly reduce to the former when the current is zero and to the latter when the bottom is flat.

Numerical results are presented in Sec. 5.1 for the scattering of waves by jet-like shearing currents in constant depth, including comparisons with the multidomain approximation method by McKee (2003), and the simplified mild-shear model(s), McKee (1987, 1996). It is shown that the present coupled-mode model with a small number of modes provides results fully compatible with the exact multidomain approximation method. Furthermore, with the aid of systematic comparisons in cases of smooth but steep shoals, in Sec. 5.2 we present and discuss the effects of transitional-type following and opposing currents on the hydrodynamic characteristics of the wave-current system.

As another interesting example, we examine in Sec. 5.3 the case of waves scattered by sinusoidal current in constant depth, and show that there are cases where strong enhancement of the wave amplitude could be obtained within downwave-directed current jets. This is in agreement with previous observations which suggested that wind-waves amplitudes might be enhanced within the downwind-directed current maxima associated with alternating ‘wind streaks’ or ‘Langmuir circulation’ (Smith 1983, 2001), leading to preferential breaking of waves along such current jets.

In Sec. 5.4 we examine the case of the wave reflection by an idealised smooth but steep underwater trench with current flowing along it. It is shown that the results obtained by the present method compare well with corresponding results by Kirby *et al* (1987) in the limiting case of an abrupt trench (with vertical walls). Finally, in Sec. 5.5, we investigate the influence of longshore-type currents over sinusoidal bottom topography on the Bragg scattering of obliquely incident water waves and discuss their effects on the shifting of the first-order resonant frequencies and the enhancement/reduction of reflection.

2. Differential formulation of the problem

The present work is based on the following differential equation on the wave pressure p , which models the combined effects of steady shearing current and variable bathymetry on small-amplitude waves, Mei (1983, Ch. 3.6, Eq. 6.17),

$$\frac{\partial^2 p}{\partial x_i \partial x_i} + \frac{\partial^2 p}{\partial z^2} = -2\rho \left(\frac{\partial u_i}{\partial x_j} \frac{\partial U_j}{\partial x_i} + \frac{\partial w}{\partial z} \frac{\partial W}{\partial z} \right), \quad (2.1)$$

where (u_1, u_2, w) denotes the wave flow, (U_1, U_2, W) denotes the steady current, $(x_1, x_2) = (x, y)$ are the horizontal coordinates and z is the vertical coordinate (positive upwards). The above equation has been obtained from the continuity equation and the Euler equations, after appropriate linearisation; see Mei (1983, Ch. 3.6, Eqs. 6.14-16). Furthermore, Eq. (2.1) is subjected to the following linearized free-surface boundary condition, Mei (1983, Eq.6.23),

$$\left(\frac{\partial}{\partial t} + U_j \frac{\partial}{\partial x_j} \right)^2 p + 2W \left(\frac{\partial p}{\partial t} + U_j \frac{\partial p}{\partial x_j} \right) - g \frac{\partial H}{\partial x_j} \frac{\partial p}{\partial x_j} + g \frac{\partial p}{\partial z} = 0, \quad \text{on } z = H, \quad (2.2)$$

where the repeated index ($j=1,2$) denotes summation with respect to this index. In Eq.(2.2), P and H denote the pressure and the free surface elevation associated with the (underlying) steady current flow, and g is the acceleration due to gravity. Furthermore, on the mean free-surface ($z=H$) the kinematic boundary condition (Mei 1983, Eq.6.21) applies:

$$\frac{\partial \eta}{\partial t} + U_i \frac{\partial \eta}{\partial x_i} + u_i \frac{\partial H}{\partial x_i} - w - \eta \frac{\partial W}{\partial z} = 0, \quad \text{on } z = H, \quad (2.3)$$

where η denotes the free-surface elevation associated with the wave. Finally, the wave pressure p must satisfy the bottom boundary condition (Mei 1983, Eq.6.19), which reads

$$\frac{\partial p}{\partial z} + \frac{\partial h}{\partial x_j} \frac{\partial p}{\partial x_j} = 0, \quad \text{on } z = -h. \quad (2.4)$$

In the present work, we consider a simplified model problem corresponding to obliquely incident harmonic waves on a horizontally non-homogeneous current in a variable-depth strip, characterized by straight and parallel bottom contours; see Fig.1. The liquid is assumed to be homogeneous, and the flow associated with the current is parallel to the bottom contours and it is considered to be steady and known. More specifically, the bottom surface exhibits an arbitrary 1D variation in a subdomain of finite length (i.e. the

bathymetry is characterised by straight and parallel bottom contours) lying between two regions of constant but possibly different depth, $h = h_1$ (region of incidence) and $h = h_3$ (region of transmission). A Cartesian coordinate system is introduced, with its origin at some point on the mean water level (in the variable bathymetry region), the z -axis pointing upwards and the y -axis being parallel to the bottom contours. The function $h(x)$ represents the local depth, measured from the mean water level. It is considered to be a smooth function, such that $h(x) = h(a) = h_1$, for $x \leq a$, and $h(x) = h(b) = h_3$, for $x \geq b$. The vertical strip D is decomposed to three subdomains $D^{(i)}$, $i = 1, 2, 3$, where $D^{(1)}$ and $D^{(3)}$ are half-strips, corresponding to $x < a$ and $x > b$, respectively, and $D^{(2)}$ is the variable bathymetry subdomain lying between $D^{(1)}$ and $D^{(3)}$. Without loss of generality, we assume $h_1 > h_3$. The same decomposition is also applied to the free-surface ∂D_F and the bottom ∂D_B boundaries. Finally, we define the vertical interfaces $\partial D_I^{(12)}$ and $\partial D_I^{(23)}$ separating the three subdomains. The latter are vertical segments (between the bottom and the mean water level) at $x = a$ and $x = b$, respectively.

We consider the scattering problem of obliquely incident plane waves, under the combined effects of variable bathymetry and the horizontally non-homogeneous shear current, $U_1 = W = 0$, $U_2 = U(x)$, existing only in $x > a$; see Fig.1. The steady current set-down is assumed to be negligible ($H=0$), and thus, also $P=0$. The current velocity is described by the continuous function $U(x)$, which can be general in the intermediate region, $a \leq x \leq b$, as, e.g., a monotonic one or a periodic one with characteristic length L . Outside this region, the current is assumed to be uniform (or simply zero),

$$U(x) = U_1 = 0, \quad x \leq a, \quad U(x) = U_3, \quad x \geq b. \quad (2.5)$$

Thus, both $U(x)$ and $h(x)$ are assumed to be smooth functions, attaining constant (but possibly different) values at the ends $x=a$ and $x=b$ of the variable bathymetry region. Restricting ourselves to monochromatic (harmonic) waves of absolute frequency ω , propagating with direction θ_1 with respect to the bottom contours in the region of incidence, the wave pressure is expressed in the form, Smith (1983, 1987),

$$p(x, y, z; t) = \text{Re} \left\{ p(x, z) \exp(i(qy - \omega t)) \right\}, \quad (2.6)$$

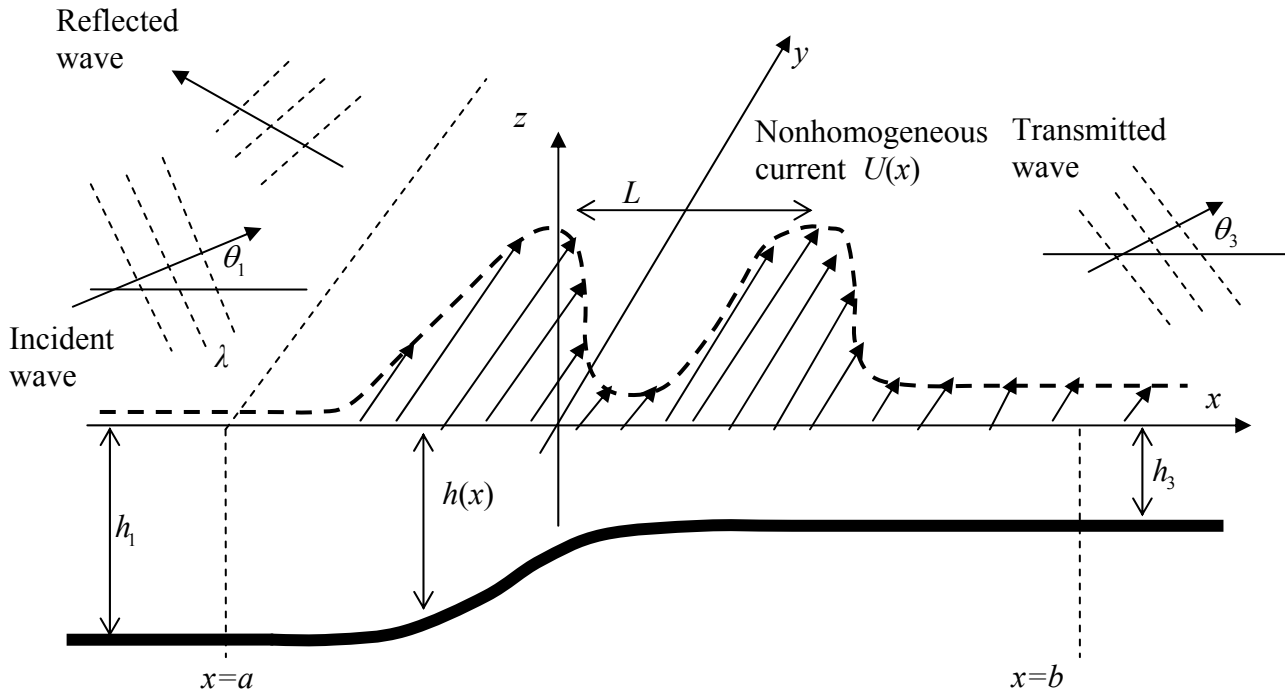


Figure 1. Geometrical configuration and basic notation

where q is the periodicity constant along the y -direction and $i = \sqrt{-1}$. Under the previous assumptions, from Eqs. (2.1), (2.2), (2.4) we obtain that the wave flow is governed by the following equation with respect to the (complex) pressure $p(x, z)$ in D ,

$$\frac{\partial^2 p}{\partial x^2} + \frac{\partial^2 p}{\partial z^2} - q^2 p + \frac{2q}{\sigma} \frac{\partial U}{\partial x} \frac{\partial p}{\partial x} = 0, \quad (2.7a)$$

subjected to the boundary conditions

$$\frac{\partial p}{\partial z} - \mu(x) p = 0, \quad \text{on } z = 0, \quad (2.7b)$$

$$\frac{\partial p}{\partial z} + \frac{dh}{dx} \frac{\partial p}{\partial x} = 0, \quad \text{on } z = -h(x), \quad (2.7c)$$

where $\sigma = \sigma(x) = \omega - qU(x)$ is the local intrinsic frequency and $\mu = \sigma^2/g$ is the corresponding frequency parameter. Following Eq. (2.3), the free-surface elevation can be obtained from the solution of the above problem as follows

$$\eta(x, y; t) = \text{Re} \left\{ \frac{p(x, z=0)}{\rho g} \exp(-i(qy - \omega t)) \right\}, \quad (2.8)$$

where ρ is the (constant) liquid density. Other quantities of interest, as, e.g., the wave velocities, can be obtained in terms of $p(x, z)$ and its spatial derivatives from the linearized Euler equations (Mei 1983, Eqs. 6.15 and 6.16) as follows:

$$u_1 = -\frac{i}{\rho\sigma} \frac{\partial p}{\partial x}, \quad u_2 = -\frac{iq}{\rho\sigma} p - \frac{1}{\rho\sigma^2} \frac{\partial U}{\partial x} \frac{\partial p}{\partial x}, \quad w = -\frac{i}{\rho\sigma} \frac{\partial p}{\partial z}. \quad (2.9)$$

The problem of water-wave scattering by the shearing current $U(x)$, with the effects of variable bathymetry, can be formulated as a transmission problem in the bounded subdomain $D^{(2)}$, with the aid of the following general representations of the pressure $p(x, z)$ in the semi-infinite strips $D^{(1)}$ and $D^{(3)}$ (Smith 1983, 1987, Kirby *et al* 1987):

$$p^{(1)}(x, z) = \left(A_0 \exp(ik_0^{(1)}x) + A_R \exp(-ik_0^{(1)}x) \right) Z_0^{(1)}(z) + \sum_{n=1}^{\infty} C_n^{(1)} Z_n^{(1)}(z) \exp(k_n^{(1)}(x-a)) \quad \text{in } D^{(1)}, \quad (2.10a)$$

where A_0 is the amplitude of the incident wave which is assumed to be known, and

$$p^{(3)}(x, z) = A_T \exp(ik_0^{(3)}x) Z_0^{(3)}(z) + \sum_{n=1}^{\infty} C_n^{(3)} Z_n^{(3)}(z) \exp(k_n^{(3)}(b-x)), \quad \text{in } D^{(3)}. \quad (2.10b)$$

The above expansions are obtained from the eigensolutions of the modified Helmholtz equation to which (2.7a) reduces in $D^{(1)}$ and $D^{(3)}$ (since $dU/dx = 0$ there). The terms $\left(A_0 \exp(ik_0^{(1)}x) + A_R \exp(-ik_0^{(1)}x) \right) Z_0^{(1)}(z)$ and $A_T \exp(ik_0^{(3)}x) Z_0^{(3)}(z)$ in the series (2.10) are the *propagating modes*, associated with incident wave (which is considered to be known), the reflected and the transmitted wave, respectively. The remaining terms ($n=1, 2, \dots$) are the *evanescent modes*. In the expansions (2.10) the horizontal wavenumbers $k_n^{(l)}$, $l=1, 3$, are defined as follows

$$k_0^{(l)} = \sqrt{\left(\kappa_0^{(l)} \right)^2 - q^2}, \quad k_n^{(l)} = \sqrt{\left(\kappa_n^{(l)} \right)^2 + q^2}, \quad n \geq 1, \quad (2.11a)$$

where $\{i\kappa_0^{(l)}, \kappa_n^{(l)}, n=1, 2, \dots\}$, $l=1, 3$, are obtained as the roots of the dispersion relations (formulated at the depths h_l , $l=1, 3$):

$$\mu_l h_l = -\kappa^{(l)} h_l \tan(\kappa^{(l)} h_l), \quad l=1, 3. \quad (2.11b)$$

In the above equations $\mu_l = \sigma_l^2 / g$, $\sigma_l = \omega - qU_l$, $l = 1, 3$. Also, the functions $\{Z_n^{(l)}(z), n = 0, 1, 2, \dots\}$ appearing in Eqs. (2.10) are given by

$$Z_0^{(l)}(z) = \frac{\cosh(\kappa_0^{(l)}(z + h_l))}{\cosh(\kappa_0^{(l)}h_l)}, \quad Z_n^{(l)}(z) = \frac{\cos(\kappa_n^{(l)}(z + h_l))}{\cos(\kappa_n^{(l)}h_l)}, \quad n = 1, 2, \dots, \quad l = 1, 3. \quad (2.12)$$

Since the current is assumed to be zero in $D^{(1)}$, the intrinsic and absolute frequencies are equal there ($\sigma = \omega$). Thus, the periodicity constant q is obtained from the wavenumber of the incident wave, as follows

$$q = \kappa_0^{(1)} \sin \theta_1. \quad (2.12)$$

where $i\kappa_0^{(1)}$ is the unique imaginary-positive root of Eq. (2.11b) for $l=1$. Then, the direction of the transmitted wave in $D^{(3)}$ is calculated by

$$\theta_3 = \sin^{-1}(\kappa_0^{(1)} \sin \theta_1 / \kappa_0^{(3)}). \quad (2.13)$$

where $i\kappa_0^{(3)}$ is the unique imaginary-positive root of Eq. (2.11b) for $l=3$.

Given the representations (2.10), the problem can be reformulated as a transmission boundary value problem for the pressure $p^{(2)}(x, z)$ in the bounded subdomain $D^{(2)}$, consisting of the following equations, boundary and matching conditions:

$$\frac{\partial^2 p^{(2)}}{\partial x^2} + \frac{\partial^2 p^{(2)}}{\partial z^2} - q^2 p^{(2)} + \frac{2q}{\sigma(x)} \frac{\partial U}{\partial x} \frac{\partial p^{(2)}}{\partial x} = 0, \quad (x, z) \in D^{(2)}, \quad (2.14a)$$

$$\frac{\partial p^{(2)}}{\partial z} - \mu(x) p^{(2)} = 0, \quad z = 0, \quad (2.14b)$$

$$\frac{\partial p^{(2)}}{\partial z} + \frac{dh}{dx} \frac{dp^{(2)}}{dx} = 0, \quad z = -h(x), \quad (2.14c)$$

$$p^{(2)} = p^{(1)}, \quad \frac{\partial p^{(2)}}{\partial x} = \frac{\partial p^{(1)}}{\partial x}, \quad x = a, \quad -h_1 < z < 0, \quad (2.14d,e)$$

$$p^{(2)} = p^{(3)}, \quad \frac{\partial p^{(2)}}{\partial x} = \frac{\partial p^{(3)}}{\partial x}, \quad x = b, \quad -h_3 < z < 0. \quad (2.14f,g)$$

In the next section we shall present a new variational principle equivalent to the transmission problem (2.14). This principle will be used in Sec. 4 to derive a new coupled-mode system governing the scattering of waves by horizontally shear current in variable bathymetry regions.

3. Variational formulation

For simplicity in the presentation, from now on we will use $p(x, z)$ to denote $p^{(2)}(x, z)$ in the bounded subdomain $D^{(2)}$. The problem (2.14) admits an equivalent variational formulation, which will serve as the basis for the derivation of the coupled-mode system of horizontal equations. Consider the functional:

$$\begin{aligned} \mathcal{F}\left(p, A_R, \{C_n^{(1)}\}_{n \in N}, A_T, \{C_n^{(3)}\}_{n \in N}\right) &= \frac{1}{2} \int_{D^{(2)}} \left(\nabla \left(\frac{p}{\sigma} \right) \right)^2 + \left(q^2 + \sigma \frac{\partial^2 \sigma^{-1}}{\partial x^2} \right) \left(\frac{p}{\sigma} \right)^2 dx dz \\ &\quad - \frac{1}{2} \int_{\partial D_F^{(2)}} \mu \left(\frac{p}{\sigma} \right)^2 dS - \frac{1}{2} \int_{\partial D_H^{(2)}} \left(\sigma \frac{\partial}{\partial n} \left(\frac{1}{\sigma} \right) \right) \left(\frac{p}{\sigma} \right)^2 dS \\ &\quad + \frac{1}{\sigma_a^2} \int_{\partial D_I^{(12)}} \left(p - \frac{1}{2} p^{(1)} \right) \frac{\partial p^{(1)}}{\partial x} dS - \frac{1}{\sigma_b^2} \int_{\partial D_I^{(23)}} \left(p - \frac{1}{2} p^{(3)} \right) \frac{\partial p^{(3)}}{\partial x} dS - A_0 A_R J^{(1)}. \end{aligned} \quad (3.1)$$

In the above equation, $J^{(1)} = 2k_0^{(1)} \int_{z=-h_1}^{z=0} \left(Z_0^{(1)}(z) \right)^2 dz$, $\sigma_a = \sigma(x=a)$ and $\sigma_b = \sigma(x=b)$,

$\partial/\partial n$ denotes the outward normal derivative on the boundary and $\nabla = (\partial/\partial x, \partial/\partial z)$.

The functions $p^{(l)}$ and their derivatives $\partial p^{(l)}/\partial x$, $l=1,3$, appearing in Eq. (3.1), are considered to be represented by means of their series expansions, Eqs. (2.10), and their horizontal derivatives, respectively.

The function $p = p^{(2)}(x, z)$, $(x, z) \in D^{(2)}$ and the coefficients $A_R, \{C_n^{(1)}\}_{n \in N}$ and $A_T, \{C_n^{(3)}\}_{n \in N}$ constitute a solution of the problem, if they render the functional \mathcal{F} stationary,

$$\delta \mathcal{F}\left(p, A_R, \{C_n^{(1)}\}, A_T, \{C_n^{(3)}\}\right) = 0. \quad (3.2)$$

As shown in Appendix A, by calculating the first variation δF of the above functional the variational equation (3.2) takes the form:

$$\begin{aligned} \delta \mathcal{F} &= - \int_{D^{(2)}} \frac{1}{\sigma^2} \left(\nabla^2 p - q^2 p + \frac{2q}{\sigma} \frac{\partial U}{\partial x} \frac{\partial p}{\partial x} \right) \delta p dx dz + \int_{x=a}^{x=b} \frac{1}{\sigma^2} \left(\frac{\partial p}{\partial z} - \mu p \right) \delta p dx - \int_{x=a}^{x=b} \frac{1}{\sigma^2} \left(\frac{\partial p}{\partial z} + \frac{dh}{dx} \frac{\partial p}{\partial x} \right) \delta p dx + \\ &\quad - \frac{1}{\sigma_a^2} \int_{z=-h_1}^{z=0} \left(\frac{\partial p}{\partial x} - \frac{\partial p^{(1)}}{\partial x} \right) \delta p dz + \frac{1}{\sigma_b^2} \int_{z=-h_3}^{z=0} \left(\frac{\partial p}{\partial x} - \frac{\partial p^{(3)}}{\partial x} \right) \delta p dz + \\ &\quad + \frac{1}{\sigma_a^2} \int_{z=-h_1}^{z=0} \left(p - p^{(1)} \right) \delta \left(\frac{\partial p^{(1)}}{\partial x} \right) dz - \frac{1}{\sigma_b^2} \int_{z=-h_3}^{z=0} \left(p - p^{(3)} \right) \delta \left(\frac{\partial p^{(3)}}{\partial x} \right) dz = 0. \end{aligned} \quad (3.3)$$

The proof of the equivalence of the variational equation (3.3) and the transmission problem (2.14) is finally obtained by using standard arguments of the Calculus of Variations (see, e.g., Rectorys 1977).

4. The Coupled-Mode System (CMS)

In this section we shall present a new coupled-mode system modelling the scattering of waves by horizontally shear current in variable bathymetry regions. The CMS is derived from the variational principle (3.3) on the basis of the following enhanced local-mode series representation of the wave pressure field in the variable bathymetry region $D^{(2)}$ (where also the current velocity $U(x)$ is varying):

$$p(x, z) = P_{-1}(x)Z_{-1}(z; x) + P_0(x)Z_0(z; x) + \sum_{n=1}^{\infty} P_n(x)Z_n(z; x). \quad (4.1)$$

The above representation has been first introduced and studied by Athanassoulis & Belibassakis (1999) for the propagation of water waves over variable bathymetry regions. In Eq. (4.1) the term $P_0(x)Z_0(z; x)$ is the propagating mode of the wave pressure field and the remaining terms $P_n(x)Z_n(z; x)$, $n=1, 2, \dots$ are the evanescent modes. The additional term $P_{-1}(x)Z_{-1}(z; x)$ is a correction term called the sloping-bottom mode, which properly accounts for the satisfaction of the bottom boundary condition on the sloping parts of the bottom, and identically vanishes on the horizontal parts of the bottom. The function $Z_n(z; x)$ represents the vertical structure of the n -th mode. The function $P_n(x)$ describes the horizontal pattern of the n -th mode and is called the complex amplitude of the n -th mode. The functions $Z_n(z; x)$, $n=0, 1, 2, \dots$, appearing in Eq. (4.1) are obtained as the eigenfunctions of the following local vertical Sturm-Liouville problem,

$$\frac{d^2 Z_n(z)}{dz^2} + \kappa_n^2 Z_n(z) = 0, \quad \text{in the interval } -h(x) < z < 0, \quad (4.2a)$$

$$\frac{dZ_n(z=0)}{dz} - \mu(x)Z_n(z=0) = 0, \quad \text{at } z = 0. \quad (4.2b)$$

$$\frac{dZ_n(z=-h)}{dz} = 0, \quad \text{at } z = -h(x), \quad (4.2c)$$

and are given by

$$Z_0(z; x) = \frac{\cosh[\kappa_0(x)(z+h(x))]}{\cosh(\kappa_0(x)h(x))}, \quad Z_n(z; x) = \frac{\cos[\kappa_n(x)(z+h(x))]}{\cos(\kappa_n(x)h(x))}, \quad n=1, 2, \dots, \quad (4.3a)$$

where the eigenvalues $\{i\kappa_0(x), \kappa_n(x)\}$ are obtained as the roots of the local dispersion relation (formulated at the local depth $h(x)$ and for the local frequency parameter $\mu(x)$):

$$\mu(x)h(x) = -\kappa(x)h(x)\tan[\kappa(x)h(x)], \quad \text{in } a \leq x \leq b, \quad \text{where } \mu(x) = \sigma^2(x)/g. \quad (4.3b)$$

A specific convenient form of the function $Z_{-1}(z; x)$ associated with the sloping bottom mode is given by

$$Z_{-1}(z; x) = h(x) \left[\left(\frac{z}{h(x)} \right)^3 + \left(\frac{z}{h(x)} \right)^2 \right], \quad (4.4)$$

and all numerical results presented in this work are based on this choice. However, other choices are also possible (see Athanassoulis & Belibassakis 1999, Sec.4). From Eqs. (4.1), (4.2c) and (4.4), we easily obtain that the sloping-bottom mode satisfies:

$$P_{-1}(x) = \frac{\partial p(x, z = -h(x))}{\partial z}, \quad (4.5)$$

and thus, it is needed only in subareas where the bottom surface is not flat. This additional mode makes the series (4.1) compatible with the Neumann bottom boundary condition (2.7c) in the sloping parts of the bottom surface, while, at the same time, it significantly accelerates the convergence of the local-mode series. For more details about the role and significance of this term we refer to Athanassoulis & Belibassakis (1999, Sec. 4), where this idea is first introduced and discussed for wave propagation/diffraction problems in variable bathymetry regions. Further details about the extension of this model to 3D can be found in Belibassakis *et al* (2001).

By using the local-mode series representation (4.1) in the variational principle (3.3), in a similar way as described in Athanassoulis & Belibassakis (1999, Sec.5), the following coupled-mode system (CMS) with respect to the pressure mode amplitudes is obtained:

$$\sum_{n=-1}^{\infty} a_{mn}(x) P_n''(x) + b_{mn}(x) P_n'(x) + (c_{mn}(x) - a_{mn} q^2) P_n(x) = 0, \quad (4.6)$$

in $a < x < b$, $m = -1, 0, 1, \dots$, where a prime denotes differentiation with respect to x . The coefficients a_{mn} , b_{mn} , c_{mn} , $m, n = -1, 0, 1, 2, \dots$, of the CMS (4.6) are given by

K.A. Belibassakis: Coupled-mode model for water wave scattering by shearing currents in variable bathymetry

$$a_{mn} = \langle Z_n, Z_m \rangle = \int_{z=-h(x)}^{z=0} Z_n(z; x) Z_m(z; x) dz, \quad (4.7a)$$

$$b_{mn} = 2 \left\langle \frac{\partial Z_n}{\partial x}, Z_m \right\rangle + \frac{2q}{\sigma} \frac{dU}{dx} \langle Z_n, Z_m \rangle + \frac{dh}{dx} [Z_n Z_m]_{z=-h}, \quad (4.7b)$$

$$c_{mn} = \langle \nabla^2 Z_n, Z_m \rangle + \left\langle \frac{2q}{\sigma} \frac{dU}{dx} \frac{\partial Z_n}{\partial x}, Z_m \right\rangle + \left[\left(\frac{dh}{dx} \frac{\partial Z_n}{\partial x} + \frac{\partial Z_n}{\partial z} \right) \right]_{z=-h}. \quad (4.7c)$$

4.1 Boundary conditions for the CMS

The CMS (4.6) is supplemented by the following decoupled end-conditions at $x=a$ and $x=b$, which are obtained from the last four terms of the variational equation (3.3),

$$P_{-1}(a) = P'_{-1}(a) = 0, \quad P_{-1}(b) = P'_{-1}(b) = 0, \quad n = -1, \quad (4.8a)$$

$$P'_0(a) + ik_0^{(1)} P_0(a) = 2ik_0^{(1)} A_0 \exp(ik_0^{(1)} a), \quad P'_n(a) - k_n^{(1)} P_n(a) = 0, \quad n = 1, 2, \dots, \quad (4.8b)$$

$$P'_0(b) - ik_0^{(3)} P_0(b) = 0, \quad P'_n(b) + k_n^{(3)} P_n(b) = 0, \quad n = 1, 2, \dots, \quad (4.8c)$$

where the coefficients $k_n^{(1)}, k_n^{(3)}$, $n=0,1,2,\dots$, are defined by Eqs. (2.11a). The coefficients of the series expansions (2.10) in the two half strips are obtained from the solution of the coupled-mode system through $P_n(a), P_n(b)$, and are given by similar relations as in Athanassoulis & Belibassakis (1999, Eqs. 5.18). In particular, the coefficients A_R and A_T defining the reflection and transmission coefficients

$$K_r = A_R / A_0, \quad K_t = A_T / A_0, \quad (4.9a)$$

are obtained from the solution of the CMS (4.6) as follows:

$$A_R = \left(P_0(a) - A_0 \exp(ik_0^{(1)} a) \right) \exp(ik_0^{(1)} a), \quad A_T = P_0(b) \exp(-ik_0^{(3)} b). \quad (4.9b)$$

An important feature of the solution of the present scattering problem by means of the representation (4.1), is that it exhibits an improved rate of decay of the modal amplitudes $|P_n(x)|$ of the order $O(n^{-4})$. Thus, a small number of modes suffices to obtain a numerically convergent solution to $P(x, z)$, even for large bottom slopes and rapidly varying currents.

4.2 Simplified forms of the CMS

In the case of mild bottom topography and slow current variations the evanescent modes P_n , $n=1,2,3,\dots$, producing localised second-order effects, can be approximately disregarded. Also, due to bottom mildness the sloping-bottom mode ($n=-1$) can be neglected. In this case, the CMS (4.6) is simplified to the following one-equation, which is called the *mild-slope and shear* equation:

$$a_{00}(x)P_0''(x) + b_{00}(x)P_0'(x) + (c_{00}(x) - a_{00}q^2)P_0(x) = 0, \quad (4.10)$$

where the coefficients are

$$a_{00} = \int_{z=-h(x)}^{z=0} Z_0^2(z;x) dz = \frac{1}{2\kappa_0} \tanh(\kappa_0 h) \left(1 + \frac{2\kappa_0 h}{\sinh(2\kappa_0 h)} \right), \quad (4.11a)$$

$$b_{00} = 2 \int_{z=-h(x)}^{z=0} \frac{\partial Z_0(z;x)}{\partial x} Z_0(z;x) dz + \frac{dh}{dx} Z_0^2(z=-h(x);x) + \frac{2q}{\sigma} \frac{dU}{dx} a_{00}, \quad (4.11b)$$

$$c_{00} = \kappa_0^2 a_{00} + \int_{z=-h(x)}^{z=0} \frac{\partial^2 Z_0(z;x)}{\partial x^2} Z_0(z;x) dz + \frac{dh}{dx} \frac{\partial Z_0(z=-h(x);x)}{\partial x} + \frac{2q}{\sigma} \frac{dU}{dx} \int_{z=-h(x)}^{z=0} \frac{\partial Z_0(z;x)}{\partial x} Z_0(z;x) dz. \quad (4.11c)$$

In the above equations, the function $Z_0(z;x)$ is given by Eq. (4.3a) and κ_0 is the positive root of the dispersion relation $\mu h = \kappa_0 \tanh(\kappa_0 h)$, which is exactly Eq. (4.3b) for $n=0$. In order to illustrate the richness and validity of the present model, we will now discuss two particular forms to which Eq. (4.10) reduces, when there is no current and when the bottom is horizontal.

(i) No current ($U=0$)

In the case of wave scattering by bottom topography without current, the above model exactly reduces to the Modified Mild-Slope equation (MMS), Massel (1993), Chamberlain & Porter (1995), Miles & Chamberlain (1998). This is easily seen from the above equations, since in this case $b_{00} = a'_{00}$, and thus Eq. (4.10) becomes

$$(a_{00}(x)P_0'(x))' + (\kappa_0^2 a_{00} - K(x) - a_{00}q^2)P_0(x) = 0, \quad (4.12a)$$

where

K.A. Belibassakis: Coupled-mode model for water wave scattering by shearing currents in variable bathymetry

$$K(x) = - \int_{z=-h(x)}^{z=0} \frac{\partial^2 Z_0(z;x)}{\partial x^2} Z_0(z;x) dz - h' \frac{\partial Z_0(z=-h(x);x)}{\partial x} = K_1 h'' + \kappa_0 K_2 (h')^2, \quad (4.12b)$$

and K_1, K_2 are functions of $\kappa_0 h$, as given by Miles & Chamberlain (1998, Eqs. 1.14b,c).

(ii) Scattering by shear current in flat domain ($dh/dx=0$)

In the case of horizontal bottom, the coefficients defined by Eqs. (4.11) become

$$a_{00} = \langle Z_0, Z_0 \rangle, \quad (4.13a)$$

$$b_{00} = 2 \left\langle \frac{\partial Z_0}{\partial x}, Z_0 \right\rangle + \frac{2q}{\sigma} \frac{dU}{dx} \langle Z_0, Z_0 \rangle, \quad (4.13b)$$

$$c_{00} = \kappa_0^2 \langle Z_0, Z_0 \rangle + \left\langle \frac{\partial^2 Z_0}{\partial x^2} + \frac{2q}{\sigma} \frac{dU}{dx} \frac{\partial Z_0}{\partial x}, Z_0 \right\rangle. \quad (4.13c)$$

In this case, Eq. (4.10) can be written in the following form:

$$\left(\Gamma(x) P_0'(x) \right)' + \left(\Gamma(x) (\kappa_0^2(x) - q^2) + \Lambda(x) \right) P_0(x) = 0, \quad (4.14a)$$

where

$$\Gamma(x) = (\sigma/\omega)^{-2} a_{00}(x), \quad \text{and} \quad \Lambda(x) = \left(\frac{\sigma}{\omega} \right)^{-2} \left(\frac{2q}{\sigma} \frac{dU}{dx} \left\langle \frac{\partial Z_0}{\partial x}, Z_0 \right\rangle + \left\langle \frac{\partial^2 Z_0}{\partial x^2}, Z_0 \right\rangle \right). \quad (4.14b)$$

The above equation is the Enhanced Mild-Shear Equation (EMSE), which has been derived and studied by McKee (1996). Furthermore, on the basis of very slow current variations ($|dU/dx| \ll 1$), the coefficient $\Lambda(x)$ becomes of higher order in comparison with $\kappa_0^2 \Gamma(x)$ and can be approximately neglected ($\Lambda(x) \approx 0$). In this case, Eq. (4.14) further reduces to the Mild-Shear Equation (MSE), which has also been derived and studied by McKee (1987).

In order to investigate the validity of EMSE and MSE models, in constant depth regions, McKee (2003) has developed an ‘exact’ multidomain approximation method, which is based on piecewise constant approximation of the current velocity and on complete normal-mode expansions (of the form of the present Eqs. 2.10) in each subdomain. The final solution concerning the coefficients of these expansions is obtained by satisfying the matching conditions at the vertical interfaces (vortex sheets) separating each subdomain (see, e.g., Smith 1983, Eqs. 2.3-4, Kirby *et al* 1987, Eqs. 2.13-14). As it will

be illustrated in Sec.5.1 (below), the present CMS (4.6) results are found to be in perfect compatibility with the multidomain approximation method.

5. Numerical results and discussion

In this section we shall present numerical results obtained by the present CMS and comparisons with other models. The discrete coupled-mode system is obtained by truncating the local-mode series (4.1) to a finite number of terms,

$$p(x, z) = \sum_{n=-1}^M P_n(x) Z_n(z; x), \quad (5.1)$$

retaining a number M of evanescent modes, in addition to the propagating and the sloping-bottom modes, and by using central, second-order finite differences based on a uniform horizontal grid of N_p points to approximate the (horizontal) derivatives in Eqs. (4.6). Discrete boundary conditions are obtained from Eqs. (4.8) by using second-order forward and backward differences to approximate derivatives at the ends ($x=a$ and $x=b$). Thus, the discrete scheme is uniformly of second-order in the horizontal direction. The forcing due to the incoming wave appears only in one equation, at the left endpoint $x = a$ (see Eq. 4.8b).

5.1 Scattering of water waves by jet-like shear currents in constant depth

We first consider the case of obliquely incident waves ($\theta_1 = 45^\circ$), in constant depth ($h=\text{const}$), scattered by a jet-like current of the form:

$$U(x) = U_{\max} \exp\left(-(x/\ell)^2\right), \quad (5.2)$$

To model the above shear current profile by the present method, we use $a = -3\ell$, $b = 3\ell$ and $U_1 = U_3 = 0$. In this example taken from McKee (2003), except of the incidence wave direction (θ_1), the other important non-dimensional parameters are :

$$\varepsilon = \omega^2 \ell / g, \quad \beta = U_{\max} \omega / g, \quad S = \omega^2 h / g. \quad (5.3)$$

In Fig. 2 we present results concerning the reflection coefficient for $H=1$ (deep water conditions), $\varepsilon=1$ and various maximum current velocities U_{\max} , corresponding to β ranging in $-2 < \beta < 2$, where negative values are associated with adverse currents and positive values with following currents, respectively. The present CMS results (shown by solid line) have been obtained by using 5 totally modes ($n=0,1,2,3,4$), which were found

to be enough for numerical convergence. We recall here that in constant depth the sloping-bottom mode is zero by definition (see Eq. 4.5) and needs not to be considered. The present CMS results are found to be in perfect agreement with the ones obtained by the multidomain approximation method by McKee (2003), shown in Fig.2 by using crosses. In addition, in this figure we include the predictions for the reflection coefficient by EMSE (dashed line) and MSE (dotted line), respectively, as calculated by the present method, using only the propagating mode ($n=0$) and, in addition, by disregarding the contribution of $\Lambda(x)$ in the coefficient c_{00} (defined by Eq. 4.13c). We are able to observe in Fig.2 the enhanced performance of the EMSE vs. the MSE model, as also reported by McKee (2003). In particular, in the examined case the EMSE model accurately predicts the reflection coefficient for $\beta > -0.5$, i.e. for relatively weak adverse currents and for following currents.

As a second example, we present in Fig. 3 results concerning again the reflection coefficient for $\beta = -1$ (strong adverse jet current) and $H=0.1$ (shallow water conditions). In this case, various wave frequencies have been considered, corresponding to ε ranging in $0 < \varepsilon < 1$. Again, we note that the results obtained by the present CMS with 5 modes (shown by solid line) are found to be in perfect agreement with the ones by the multidomain approximation method, McKee (2003) shown in Fig.3 by using crosses. Furthermore, we are able to observe in this figure that the EMSE predictions (shown by using dashed line) are better than the predictions obtained by the MSE (shown by dotted line), for values of the frequency parameter in the interval $0.07 < \varepsilon < 0.85$. However, it is also seen in Fig. 3 that for very low frequencies, corresponding to $\varepsilon < 0.07$, the EMSE fails to correctly predict the reflection coefficient, producing large discrepancies. In particular, as $\varepsilon \rightarrow 0$ the EMSE erroneously predicts $K_r \rightarrow 1$.

5.2 Waves scattered by smooth underwater shoal (with and without current)

In order to illustrate the combined effects of variable bathymetry and shearing current on the wave field, we examine in this section the case of a smooth but steep underwater shoal, which is characterised by the following depth function

$$h(x) = \frac{h_1 + h_3}{2} - \frac{h_1 - h_3}{2} \tanh\left(3\pi\left(\frac{x-a}{b-a} - \frac{1}{2}\right)\right), \quad (5.4)$$

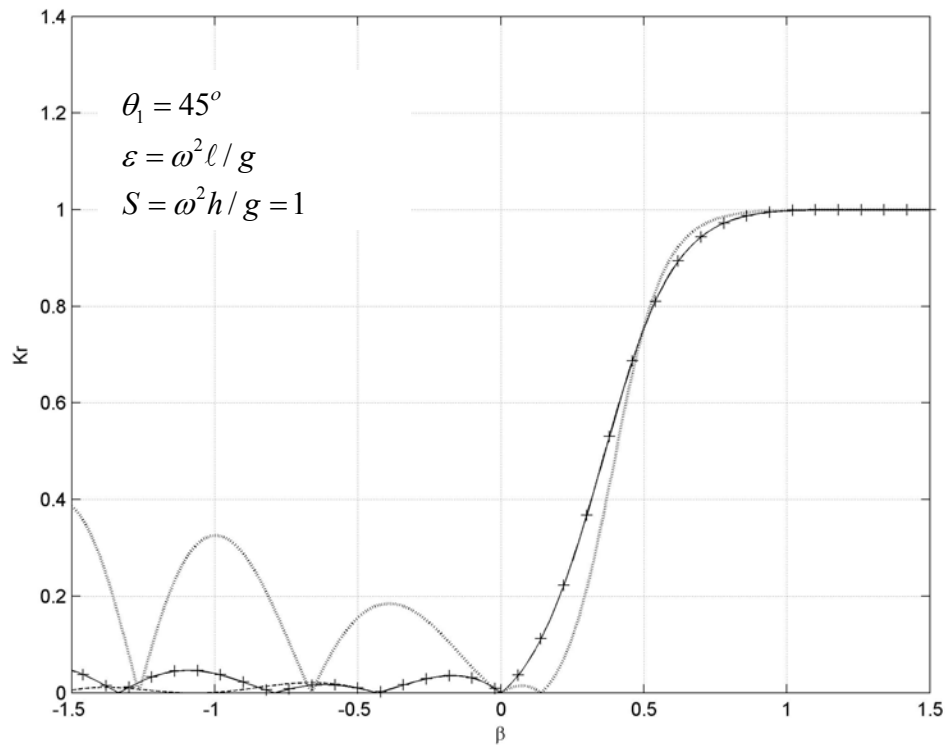


Figure 2. Obliquely incident waves scattered by opposing and following currents, in deep water. Comparison of the modulus of the reflection coefficient, as obtained by the present CMS (solid line), EMSE (dashed line) and MSE (dotted line), for various current velocities. Results obtained by the multidomain approximation method (McKee 2003) are shown by using crosses.

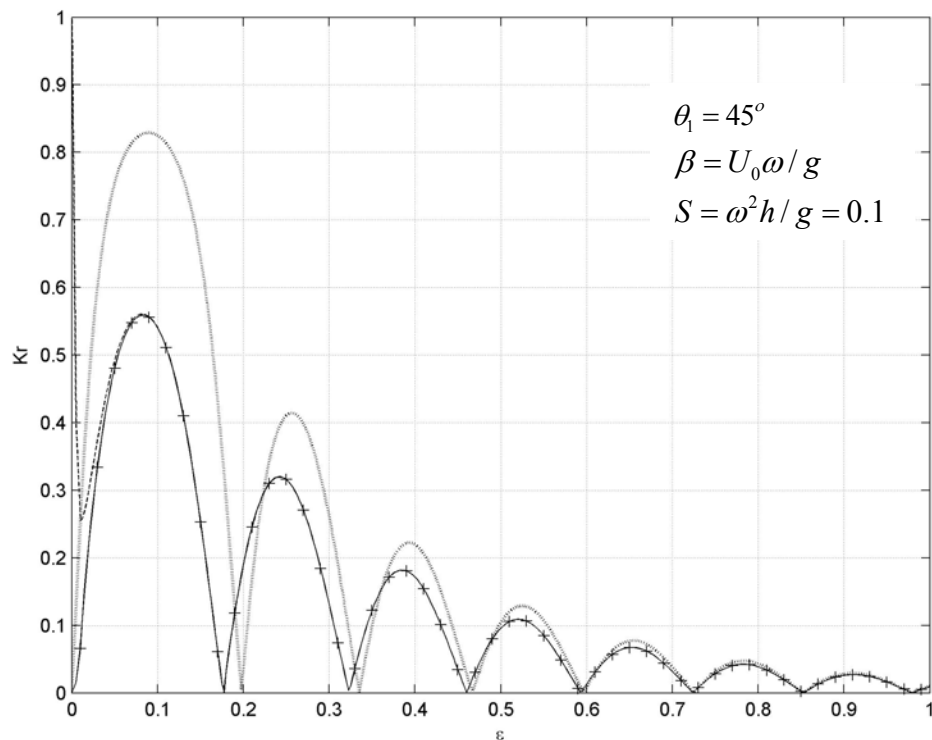


Figure 3. Obliquely incident waves scattered by opposing shear current, in shallow water. Comparison of the modulus of the reflection coefficient, as obtained by the present CMS (solid line), EMSE (dashed line) and MSE (dotted line), for various frequencies. Results obtained by the multidomain approximation method (McKee 2003) are shown by using crosses.

in $a = 0 < x < b = 20m$, with $h_1 = 15m$ and $h_3 = 5m$. This bottom profile is quite steep, having mean slope 50% and maximum slope 240%. (A sketch of the bottom topography is shown in Fig. 4). The angular frequency of the incident wave is selected to be $\omega = 1.62 \text{ rad/sec}$, corresponding to shoaling ratio $h_1 / \lambda = 0.64$, where λ is the local wavelength (that implies almost deep-water wave conditions in $D^{(1)}$), and the incident wave direction is taken to be $\theta_1 = -45^\circ$. The phase speed of the waves in the region of incidence is $c_1 = 6.06m/s$.

We first consider the case of wave scattering by bottom topography only, without any current effects. In this case, the shoaling ratio is $h_3 / \lambda = 0.235$ (implying intermediate water-depth wave conditions in $D^{(3)}$), and the corresponding phase speed of the waves in the region of transmission is $c_3 = 5.47m/s$. After passing through the variable bathymetry region the waves are refracted due to shoaling and the direction of the transmitted wave is $\theta_3 = -39.6^\circ$. In this case, the reflection and transmission coefficients, as calculated by the present CMS (4.6) using totally 5 modes ($n=-1,0,1,2,3$) and $N_p = 251$, are found to be: $K_r = 0.025$, $K_t = 0.884$. In this and similar cases that will be presented in the sequel, such a small number of retained modes in the local-mode series (4.1) is found to be enough for numerical convergence, provided that the sloping-bottom mode ($n=-1$) is included.

A contour plot of the wave field (real part of wave pressure) above the variable bathymetry domain is shown in Fig. 4. In this figure the system of isobars is shown both in the horizontal plane (upper part of the figure) and in the vertical plane (lower part). Extension of the isobars below the bottom surface has been maintained in the lower part of this figure in order to better visualise the fulfilment of the Neumann boundary condition on $z = -h(x)$, which is equivalent to the fact that the equipressure lines intersect the bottom profile perpendicularly (cf. Eq. 2.7c). Also, the distribution of the wave pressure on the free surface is plotted on the lower part of Fig.4, which is proportional to the free-surface elevation (Eq. 2.8). It is worth noticing here that in the case of no current, the present CMS is equivalent to the consistent coupled-mode model developed by Athanassoulis & Belibassakis (1999) for the propagation of waves over variable bathymetry regions results. Thus, the results presented in Fig.4 are in perfect agreement with the ones obtained by latter coupled-mode model.

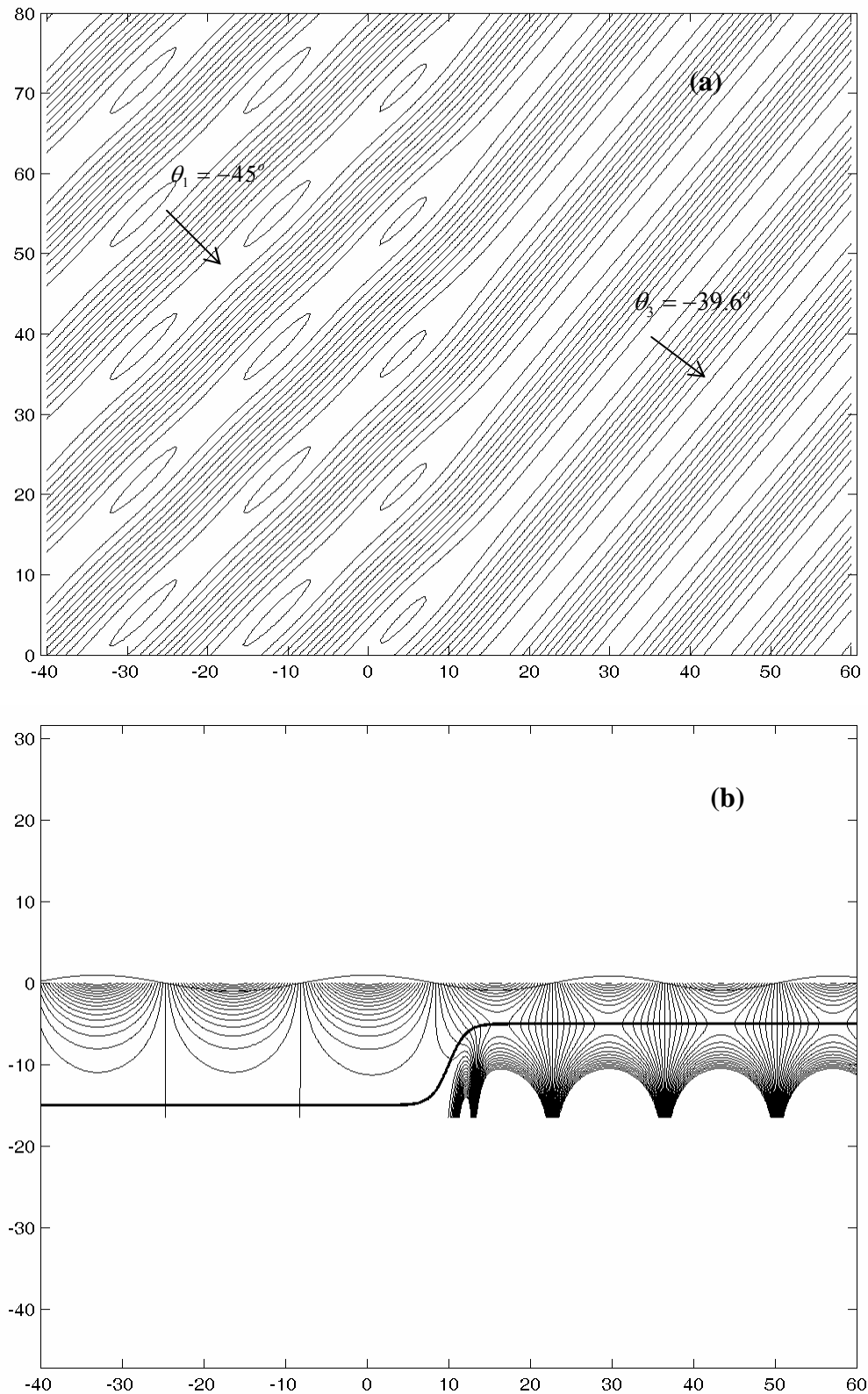


Figure 4. Refraction/diffraction of waves over a smooth but steep shoal, without the effects of current. Incident wave frequency $\omega=1.62\text{rad/s}$ and direction $|\theta_1|=45^\circ$. Plot of the wave field (a) on the horizontal plane, (b) on the vertical plane.

In Figs. 5 and 6, we present similar results for the same shoal and wave incidence as before, but with the additional effects of a following (Fig. 5) and of an opposing (Fig. 6) transitional shear current. The magnitude of the current velocity is taken to be:

$$U(x) = \frac{U_3}{2} + \frac{U_3}{2} \tanh\left(3\pi\left(\frac{x-a}{b-a} - \frac{1}{2}\right)\right), \quad (5.5)$$

in $a = 0 < x < b = 20m$. Thus, the shear current velocity varies monotonically from a minimum value $U_1 = 0$ to a maximum value U_3 , which is taken to be one quarter of the phase speed of waves in the region of incidence, $U_3 = \max U = 0.25c_1$ (where $c_1 = 6.06m/s$). Now, the wave directions in the region of transmission $D^{(3)}$ are modified due to current, and in the case of the following current $|\theta_3|$ increases, while in the case of the adverse current $|\theta_3|$ decreases, as predicted by Eq. (2.13).

To illustrate the current effects on the detailed structure of the wave pressure field, the latter is comparatively plotted in Figs. 5 and 6, on both the horizontal and vertical planes, by using contour lines. (Again, only the real part of the wave pressure field is shown). The direction and horizontal structure of the current is also schematically presented in these figures by using arrows. We observe in these figures, in comparison with the previous results with no current presented in Fig.4, the continuous variation of the wavelength (which increases for following and decreases for adverse currents), taking place in the intermediate subdomain $D^{(2)}$. In addition, in all cases we observe that the equipressure lines intersect the bottom surface perpendicularly, which is evidence of the consistent satisfaction of the Neumann bottom boundary condition, both on the horizontal and on the sloping parts of the bottom. The previous examples (Figs. 4,5,6) correspond to incident wave conditions and current velocity such that much of the wave energy penetrates the region of transmission. The main results concerning the refraction parameters, reflection and transmission coefficients are summarized in Table 1.

current type	$\max U / c_1$	$ \theta_3 $	K_r	K_t
–	0	39.6	0.025	0.884
following	0.25	57.5	0.176	0.852
opposing	-0.25	29.3	0.053	0.999

Table 1. Refraction/diffraction parameters of waves scattered by transitional current over smooth underwater shoal

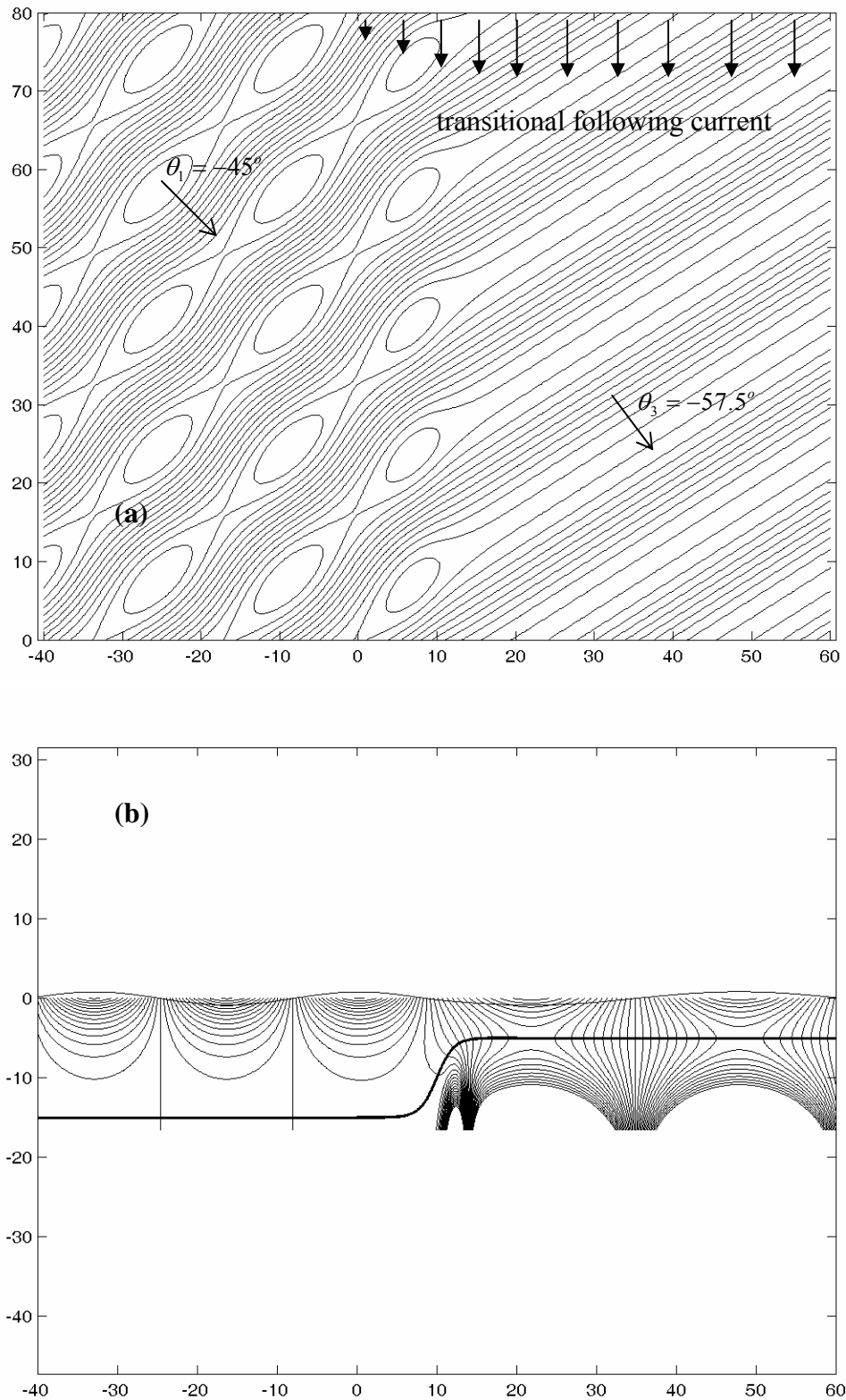


Figure 5. Refraction/diffraction of waves over a smooth and steep shoal, with the effects of a following transitional shear current. Incident wave frequency and direction same as in Fig. 4. Plot of the wave field (a) on the horizontal plane, (b) on the vertical plane.

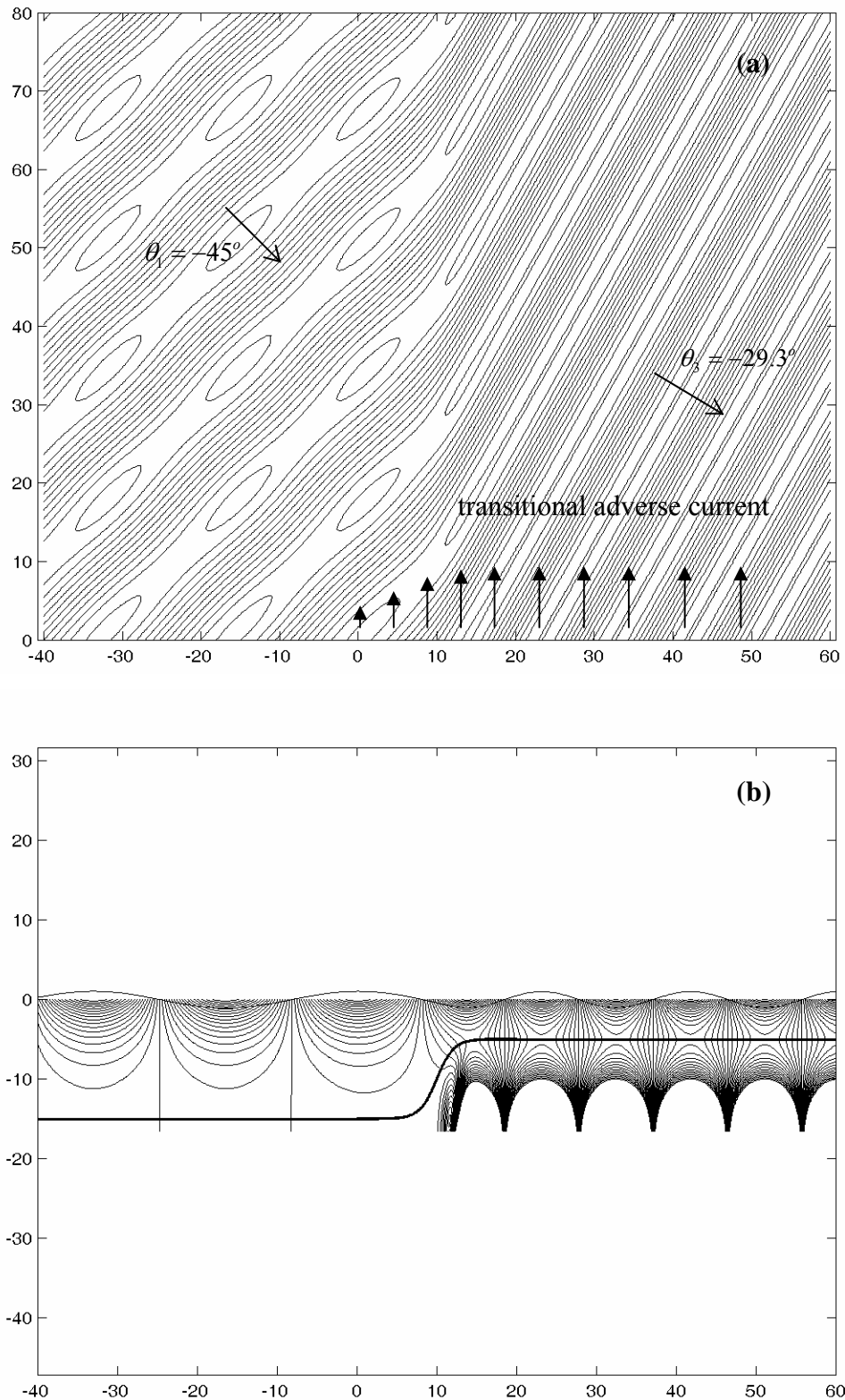


Figure 6. Refraction/diffraction of waves over a smooth and steep shoal, with the effects of an opposing transitional shear current. Incident wave frequency and direction same as in Fig. 4. Plot of the wave field (a) on the horizontal plane, (b) on the vertical plane.

5.3 The case of a sinusoidal current

It is well known that in the case of obliquely incident waves on an opposing jet-like shear current, in constant depth, wave trapping can occur under particular conditions (see, e.g. the discussion by Mei 1983, Sec.3.7.2 and Fig.7.2, and the discussion after Eq.6.22). This could lead to great amplification of the wave in a transverse channel along the current maximum. On the other hand, observations suggested that wind-waves amplitudes might be enhanced within the downwind-directed current maxima associated with alternating ‘wind streaks’ or ‘Langmuir circulation’ (see also Smith 2001), leading to preferential breaking of waves along such current jets. In order to theoretically investigate such phenomena, Smith (1983) developed an eigenfunction expansion technique for the scattering of waves in constant depth by narrow current jets, modelled by a top-hat pattern. The model problem consisted of three homogeneous subregions separated by vertical vortex sheets. However, the results indicated that wave amplitudes should be decreased within such current jets.

In order to extend the above investigation, that was restricted to single uniform current jets and shear concentrated along the edges of the jet, to the case of more complex, horizontally alternating current structure, we consider here as another example the case of waves of angular frequency $\omega = 2.2 \text{ rad/sec}$, propagating with direction $\theta_1 = 60^\circ$ in a constant depth strip $h=15\text{m}$, and scattered by a following sinusoidal shear current with horizontal profile of the form:

$$U(x) = \frac{c_1}{20} \left(1 - \cos \left(2\pi \frac{x-a}{L} \right) \right), \quad L = \frac{b-a}{2}. \quad (5.6)$$

Thus, the maximum current velocity is equal to one tenth of the phase speed of waves in $D^{(1)}$ and $D^{(3)}$, which in the present case is $c_1 = c_3 = 4.46 \text{ m/s}$. This current has the form of two streaks and is characterised by continuously distributed shear. More specifically, the shear current exists only in the region from $a=0\text{m}$ to $b=20\text{m}$ ($U_1 = U_3 = 0$), and it has a periodic horizontal structure with characteristic length $L=10\text{m}$, that is comparable to the incident wavelength ($L/\lambda = 0.78$). In addition, the wave conditions in the region of incidence correspond to deep water conditions ($h/\lambda = 1.17$).

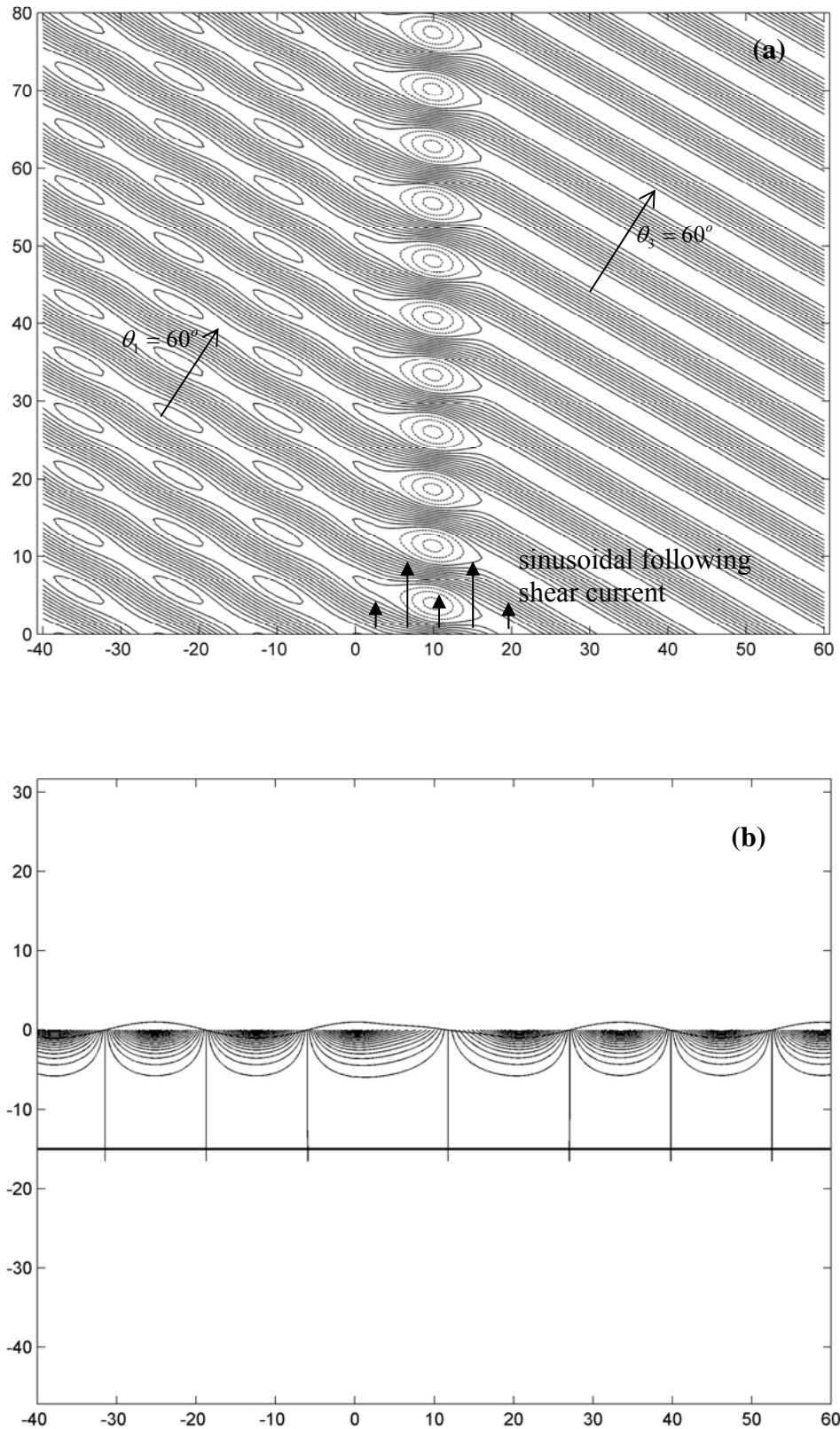


Figure 7. Refraction/diffraction of waves by a following sinusoidal current, in constant depth. Incident wave frequency $\omega=2.2\text{rad/s}$ and direction $\theta_1 = 60^\circ$. Plot of the wave field (a) on the horizontal plane, (b) on the vertical plane.

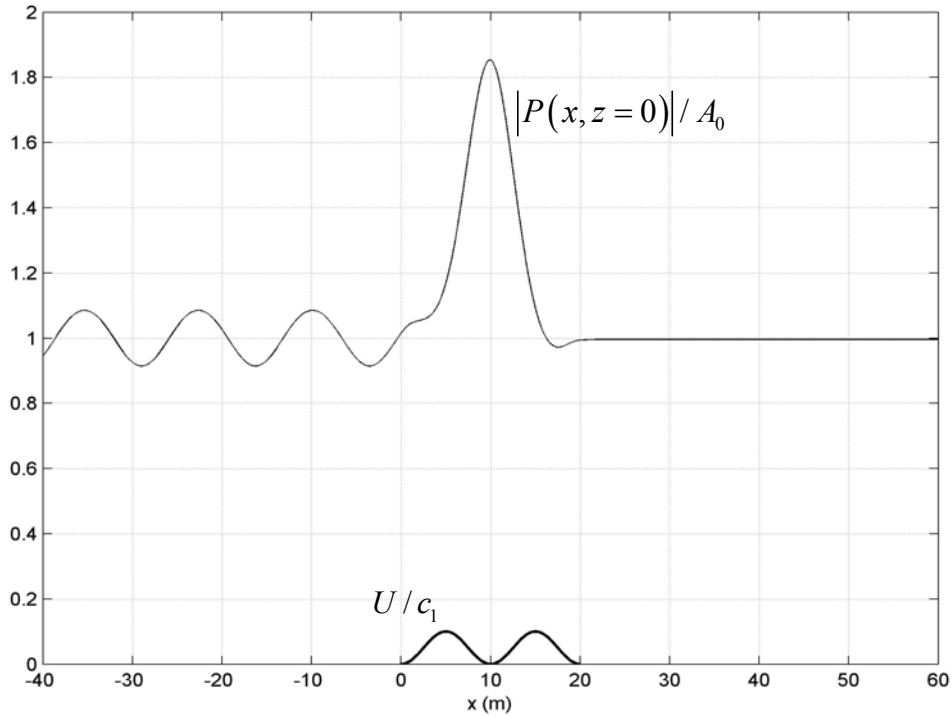


Figure 8. Amplification factor of waves scattered by a following sinusoidal current. Incident wave frequency $\omega=2.2\text{rad/s}$ and direction $\theta_1 = 60^\circ$.

The real part of the calculated wave field, as well as the distribution of the wave pressure on the free surface (which is proportional to the free-surface elevation), are shown in Fig. 7, as obtained by the present method by using only 5 modes ($n=0,1,2,3,4$) in the series (4.1) and $N_p = 251$. Again the latter have been proved enough for numerical convergence, even for such large gradients of the horizontal current velocity. We observe in the upper part of Fig.7 the formation of a transverse channel on the horizontal plane, centered at $x=10\text{m}$, associated with partial trapping of the wave energy. In Fig.8 we present the amplification factor of the wave $|P(x, z=0)|/A_0$ (where A_0 is the amplitude of the incident wave), as calculated by the present method, along with the sinusoidal current profile. Strong enhancement of the wave amplitude is observed at $x=10\text{m}$, i.e. along the central axis of the current (5.6), corresponding to more than 180% increase of the incident wave amplitude.

An explanation of the above result is possible on the basis of simple refraction principles. The incident wave direction increases within the first current jet ($0 < x < 10\text{m}$) due to increase of phase speed, as shown in Mei (1983, Fig.7.2a). Due to the fact that the

wavelength is comparable with the horizontal length of the current, the wave at the exit of from the first jet ($x = 10\text{m}$) has a local direction which is greater than 60° . The latter is such that the wave is partially reflected from the second jet, as shown in Mei (1983, Fig.7.2b). Thus, small part of wave energy returns towards the central axis of the current (5.6) and is trapped in the transverse channel. The calculated reflection and transmission coefficients by the present CMS, as also can be observed in Fig.7, are: $K_r = 0.085$, $K_t = 0.996$. Thus, almost all the wave energy penetrates the region of transmission $D^{(3)}$, and at $x > 20\text{m}$ the wave direction has recovered its initial value: $\theta_3 = \theta_1 = 60^\circ$. Consequently, repeated similar patterns of wave enhancement are expected to occur, if the alternating following current structure (5.6) is assumed to be periodically extended in $D^{(3)}$.

5.4 Scattering of waves by current flowing along a smooth underwater trench

Another interesting case that can be further investigated by means the present method concerns the propagation of obliquely incident waves over trenches with currents flowing along them. As pointed out by Kirby *et al* (1987), such phenomena could occur from waves scattered by tidal flows along natural or dredged channels, where in the latter case the presence of rigid walls may serve to guide the current and stabilize the position of boundaries in a practical sense. In order to study scattering of waves by current flowing along an abrupt underwater trench, Kirby *et al* (1987), extending previous works by Evans(1975) and Smith(1983,1987), developed and compared methods based on matched eigenfunction expansions and boundary integral equations. Again, the model problem consisted of three homogeneous subregions separated by vertical vortex sheets.

For illustrating the extending capability of the present method and the compatibility of its predictions with the analysis by Kirby *et al* (1987), we present in Fig.9 results concerning the transmission coefficient over two symmetric underwater trenches with the effects of current flowing over them. Two bottom profiles, shown in the upper part of Fig.9 with thick solid and dashed lines have been used for calculations. At the regions of incidence and transmission the depth is $h_1 = h_3 = 5\text{m}$ and at the center of the trench the maximum depth is $h_{\max} = 15\text{m}$. The corresponding depth functions have been obtained by symmetrical use of Eq.(5.4), with appropriate values of the parameters and of the

coefficient in the argument of hyperbolic tangent controlling the maximum bed steepness, which in the first case (solid line) is 94.2% and in the second (dashed line) is 188%. Also, in the upper part of Fig.9 the horizontal structure of the current flowing over the trench is shown, which in the examined case is defined by

$$U(x) = \frac{U_{\max}}{2} \left(1 - \cos \left(2\pi \frac{x-a}{b-a} \right) \right), \quad \text{in } a < x < b, \quad (5.7)$$

where $a = -50\text{m}$, $b = 50\text{m}$, and $F = U_{\max} / \sqrt{gh_{\max}}$ denotes the bathymetric Froude number associated with the maximum current velocity. The shear current exists only in the region from $a = -50\text{m}$, $b = 50\text{m}$ ($U_1 = U_3 = 0$). As it can be seen in the upper part of Fig. 9 the mean width of the trench, where also the flowing current is significant, is $L=50\text{m}$, and thus $L = 10h_1$. The situation resembles the one presented and discussed by Kirby *et al* (1987, Fig.6), with the difference that here the bathymetry and current velocity vary continuously.

In Fig. 9 we present results concerning the transmission coefficient (K_t) over the two smooth but steep underwater trenches, with the effects of current flowing over them. The incident wave direction is selected to be $\theta_1 = 45^\circ$. The present method results for various values of the nondimensional wavenumber $\kappa_1 h_1$ have been obtained by using 5 modes ($n=-1,0,1,2,3$) in the series (4.1) and $N_p = 501$. For compatibility with the analysis by Kirby *et al* (1987, Fig.6) for an abrupt underwater trench, in this example three cases have been considered, corresponding to $F = -0.05, 0, 0.05$. In the range of $\kappa_1 h_1$ from 0.1 to 0.8, 1.0, 1.3, for previous values of the Froude number, respectively, where the wave-current-seabed interaction is significant, the transmission coefficient of the smooth but steep trenches is found to be greater than the one corresponding to the abrupt trench, as it is naturally expected. Furthermore, as the trench wall steepness increases the present method results converge to ones by Kirby *et al* (1987), shown in Fig.9 by using symbols.

5.5 Longshore current effects on resonant reflection of waves by sinusoidal bathymetry

A final result presented in this work concerns the investigation of longshore current effects on the reflection of waves by sinusoidal bathymetry. The phenomenon of resonant reflection by undulating bottom topography has drawn considerable attention owing to its

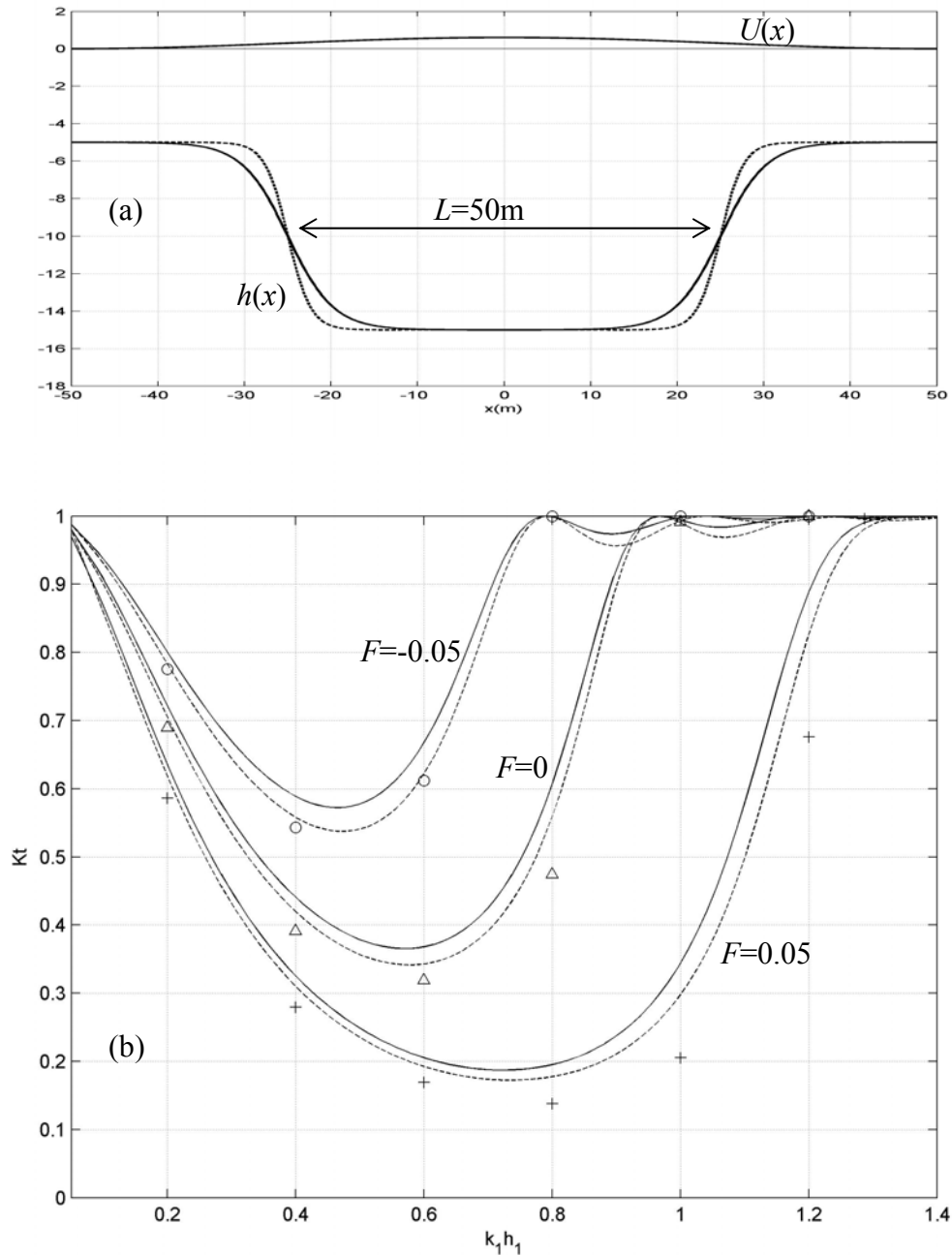


Figure 9. Wave transmission over smooth but steep symmetric trenches, for various nondimensional wavenumbers $k_1 h_1$ and bathymetric Froude numbers $F = U_{\max} / \sqrt{g h_{\max}}$, as obtained by the present CMS. (a) Bottom geometry and current profile. (b) Transmission coefficient. Solid line: smooth trench with max wall steepness 94.2%. Dashed line: smooth trench with max wall steepness 94.2%. Symbols indicate results by Kirby et al (1987, Fig6) for an abrupt underwater trench.

significant role in the evolution of nearshore waves and its possible relation to coastal morphology (development of shore-parallel bars). In addition, the existence of Bragg scattering provides a possible means for constructing coastal protection devices relatively low in profile in comparison to the waterdepth. The above remarks justify the extent of theoretical and experimental works presented on this subject by many authors (see, for example, Davies & Heathershaw 1984, Mei 1985, Dalrymple & Kirby 1986, Mei *et al* 1988, Guazzelli *et al* 1992, O'Hare & Davies 1993, Kirby 1993, Liu & Yue 1998).

However, as pointed out by Kirby (1988), any such physical formation or installation being of finite length along the longshore dimension, it is likely to result in depression of the maximum setup behind the bar that would generate a nearshore circulation pattern. This is expected to produce mean flows with onshore/offshore directions, and perhaps also with longshore component above the bar field. The effects of cross-shore current on the resonant reflection of water waves by sand bars have been studied by Kirby (1988), by using multiple-scale expansions to obtain evolution equations for the amplitudes of waves. The latter were then used to investigate the resonant reflection of waves by bar fields for both normal and oblique incidence. In order to examine the longshore shear current effects on resonant reflection of waves by sinusoidal bathymetry using the present CM, we consider the bottom topography characterised by the following depth function:

$$h(x) = h_0 - B \sin(\ell_b x), \quad \text{in } 2\pi/\ell_b < x < 2\pi(n+1)/\ell_b, \quad \text{and } h(x) = h_0 \text{ otherwise.} \quad (5.8)$$

In the above equation, ℓ_b denotes the bottom wavenumber and B the amplitude of the bottom undulations. To maintain correspondence with the experimental results presented in Davies and Heathershaw (1984), $n=4$ case, we chose $h_0 = 15.625\text{cm}$, $B/h_0 = 0.32$ and $\ell_b = 2\pi$ (so that the length of the bottom periodic cell is 1m). A plot of this bottom topography is shown in the upper part of Fig. 10. Numerical results are obtained by the present CMS using 5 totally modes ($n=-1,0,1,2,3$) and 251 gridpoints per bottom wavelength. The results concerning the reflection coefficient are shown in Fig. 10 in the following range of the resonant parameter $0.5 < 2\kappa \cos(\theta)/\ell_b < 1.8$, around the point of first-order Bragg resonance, which in the case of no current is given by

$$2\kappa \cos(\theta)/\ell_b = 1, \quad (5.9)$$

where in this subsection κ and θ will be used to denote the incident wavenumber and direction ($\kappa = \kappa_0^{(1)}$ and $\theta = \theta_1$). For comparison, in Fig. 10 we present results (always

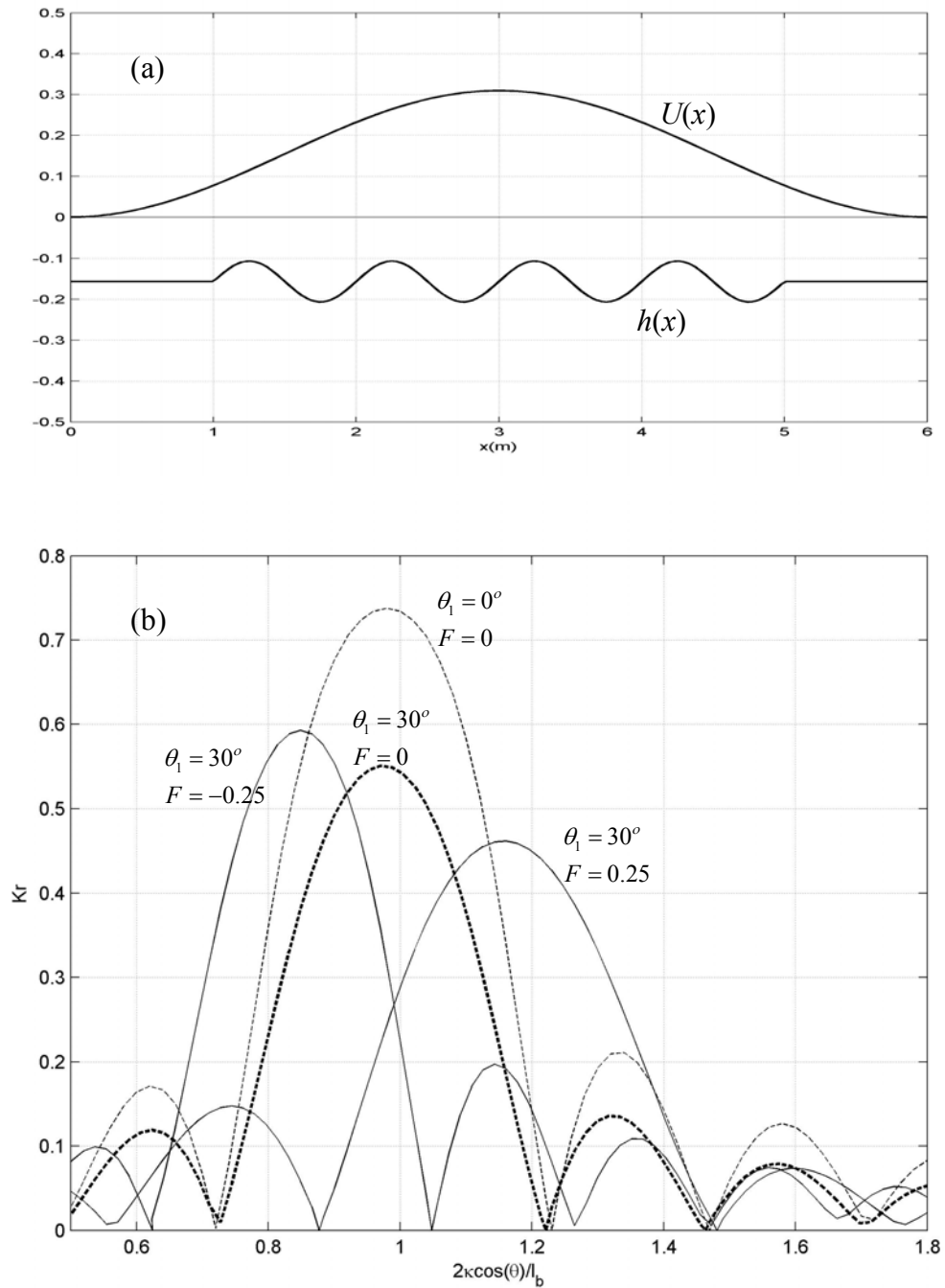


Figure 10. Wave reflection over sinusoidal bottom topography for various incidence angles θ_1 and bathymetric Froude numbers F . (a) Bottom geometry and longshore current profile. (b) Reflection coefficient.

obtained by the present CMS) for normal $\theta = 0^\circ$ and oblique $\theta = 30^\circ$ incidence, without current (shown by dashed lines), and for oblique incidence $\theta = 30^\circ$ with the effects of following and opposing jet-like currents. The current profile is of the form of Eq. (5.7), with $a = 0\text{m}$, $b = 6\text{m}$ (and is shown in Fig.10(a) by using solid lines). In order to better illustrate the current effects, relatively strong velocities have been considered, corresponding to bathymetric Froude numbers $F = U_{\max} / \sqrt{gh_0} = \pm 0.25$.

In the case of no current, the present method results, shown by dashed lines in Fig.10(b), are found to be in very good agreement with corresponding predictions by other theoretical models and with experimental data; cf. O'Hare & Davies (1993, Fig.3b), in the case of normal incidence, and Kirby (1993, Fig.5), in the case of oblique incidence. We observe in Fig. 10 that the peak of the main lobe of the reflection coefficient (K_r) is located at $2\kappa \cos(\theta) / \ell_b \approx 0.98$, i.e. slightly shifted to lower value of the resonance parameter than the one predicted by Eq. (5.9).

The Doppler shift of frequency due to the current, also shifts the position of the peak of the main lobe of K_r from $2\kappa \cos(\theta) / \ell_b \approx 1$, for $F = 0$, to much lower value $2\kappa \cos(\theta) / \ell_b \approx 0.84$ in the case of opposing current ($F = -0.25$), and to higher value $2\kappa \cos(\theta) / \ell_b \approx 1.16$ in the case of following current ($F = 0.25$). The above differences (-0.14 and 0.18, respectively) in the values of the resonant parameter $2\kappa \cos(\theta) / \ell_b$ controlling the location of the main the peak of K_r can be predicted, at a first order of approximation, by using the dispersion relation formulated at $F=0$ to obtain the variation of wavenumber in the neighbourhood of the K_r -peak due to frequency shift :

$$\Delta\kappa = \frac{1}{C_g}(\sigma - \omega) = -\frac{qU_{\max}}{C_g} = -\frac{\kappa \sin(\theta)U_{\max}}{C_g}, \quad (5.10)$$

where $C_g = d\omega/dk$ denotes the group velocity calculated at $\kappa = \ell_b / 2 \cos(\theta)$ without taking into account any current effects. Using Eq. (5.10) for $\kappa = \ell_b / 2 \cos(\theta)$, in conjunction with the resonance condition, which now reads

$$2(\kappa + \Delta\kappa) \cos(\theta) / \ell_b = 1, \quad (5.11)$$

we obtain the following result

$$2\kappa \cos(\theta) / \ell_b = 1 \pm \varepsilon. \quad (5.12a)$$

In the above equation the plus sign refers to following current and the minus sign to opposing current, respectively, and

$$\varepsilon = \frac{2|\Delta\kappa|\cos(\theta)}{\ell_b} = \frac{2\sin(\theta)}{P} F \left(\frac{2\cos(\theta)}{\ell_b h} \tanh\left(\frac{\ell_b h}{2\cos(\theta)}\right) \right)^{-1/2}, \quad (5.12b)$$

where $P = 1 + \frac{\ell_b h / \cos(\theta)}{\sinh(\ell_b h / \cos(\theta))}$. Application of the above formula to the examined case

results in $\varepsilon = 0.145$. Thus, Eq. (5.12) predicts the location of the main-lobe peak at $2\kappa \cos(\theta) / \ell_b = 1 \pm 0.145$ which is found to approximate well the real values 0.84 and 1.16, respectively.

Furthermore, we observe in Fig. 10 that in the examined wave incidence $\theta = 30^\circ$, the shape of the main lobe of K_r , for $F = \pm 0.25$ looks similar to the one for $F = 0$. However, the main lobe is $\sim 9\%$ narrower in the case of opposing current, and $\sim 19\%$ broader in the case of following current, in comparison with the no current case ($F = 0$). Also, the peak value of K_r appears to be $\sim 10\%$ greater for $F = -0.25$, and $\sim 18\%$ lower for $F = 0.25$. Thus, it seems that the area under the main lobe of the reflection coefficient is approximately conserved for symmetric jet-like currents. The above results and remarks could be found useful for extending analytical models for the approximate prediction of the reflection coefficient around the position of the peak of the main lobe (as e.g., the ones given by Mei *et al* 1988 and Kirby 1993) to the case of Bragg scattering by sinusoidal bottom in the presence of longshore shear currents, at least for low angles of wave incidence where the K_r pattern is less complex (see, e.g., Kirby 1993, Fig.5).

5 . Conclusions

A continuous coupled-mode method has been developed for wave-current-seabed interaction in variable bathymetry regions, with application to the problem of wave scattering by steady shearing currents, characterised by current variations on various scales. The present method does not introduce any simplifying assumptions or other restrictions concerning the bottom slope and curvature or the horizontal gradient of the current. Based on a variational principle, in conjunction with a rapidly-convergent local-mode series expansion of the wave pressure field in a finite subregion containing the current variation and the bottom irregularity, a new coupled-mode system of equations is obtained, governing the scattering of waves in the presence of variable bathymetry and longshore shearing currents.

In addition, by keeping only the propagating mode in the local-mode series, a new one-equation model has been derived, called the *mild slope and shear equation*, having the property to reduce to modified mild-slope equation when current is zero and to the enhanced mild-shear equation when the bottom is flat.

Finally, the analytical structure of the present model facilitates its extension to various directions as: (i) to three-dimensional problems, (ii) to treat wave scattering by more complex current systems, characterized by more general vertical structure with cross-jet component, and (iii) to include the effects of weak nonlinearity.

REFERENCES

- ATHANASSOULIS, G.A. & BELIBASSAKIS, K.A. 1999 A consistent coupled-mode theory for the propagation of small-amplitude water waves over variable bathymetry regions. *J. Fluid. Mech.*, **389**, 275-301.
- BELIBASSAKIS, K.A., ATHANASSOULIS, G.A. & GEROSTATHIS Th. 2001 A coupled-mode model for the refraction-diffraction of linear waves over steep three-dimensional bathymetry. *Applied Ocean Res.* **23** (6), 319-336.
- BERKHOFF, J.C.W. 1972 Computation of combined refraction-diffraction. *Proceedings of the 13th Int. Conf. on Coastal Engineering*, pp. 796-814, ASCE.
- BOOIJ, N., 1981 Gravity waves on water with non-uniform depth and current. *Rep.* 81-1, Delft Univ. of Technology.
- CHAMBERLAIN, P.G. & PORTER, D. 1995 The modified mild-slope equation. *J. Fluid Mech.* **291**, 393-407.
- CHEN, W., PANCHANG V. & DEMIRBILEK, Z., 2005 On the modeling of wave-current interaction using the elliptic mild-slope wave equation. *Ocean Engineering* **32** (17-18), 2135-2164.
- DALRYMPLE, R. A. & KIRBY, J. T. 1986 Water waves over ripples. *J. Waterways, Port, Coastal Ocean Engng* **112**, 309-319.
- DAVIES, A.G & HEATHERSHAW, A.D. 1984 Surface-wave propagation over sinusoidal varying topography. *J. Fluid Mechanics* **144**, 419-433.
- DYSTHE, K.B. 2000 Modelling a Rogue Wave – Speculations or a realistic possibility. In M. Olagnon & G. Athanassoulis (eds.) *Rogue Waves 2000*, pp. 255-264, Editions Ifremer, Plouzane, France.
- ECKART, G. 1952 The propagation of gravity waves from deep to shallow water. In *Gravity Waves: (Proc. NBS Semicentennial Symp. on Gravity Waves, June 15-18, 1951)*, pp 156-175. Washington: National Bureau of Standards.
- EVANS, D.V. 1975 The transmission of deep-water waves across a vortex sheet. *Journal of Fluid Mechanics* **68**, 389-401.
- FAULKNER, D. 2000 Rogue Waves – defining their characteristics for marine design. In M. Olagnon & G. Athanassoulis (eds.), *Rogue Waves 2000*, pp. 3-18, Editions Ifremer, Plouzane, France.

- GUAZZELI, E., REY, V. & BELZONS, M. 1992 Higher-order Bragg reflection of gravity surface waves by periodic beds *J. Fluid Mechanics*, **245**, 301-317.
- JONSSON, I.G. 1990 Wave-current interactions. In B. LeMehaute & D.M. Hanes (eds.) *The Sea*, 9(a), Ocean Eng. Sc., pp. 65-120, John Wiley, New York.
- KIRBY, J.T. 1984 A note on linear surface wave-current interaction over slowly varying topography. *J. Geophys. Res.*, **89**, 745-74
- KIRBY, J.T. 1988 Current effects on resonant reflection of surface water waves by sand bars. *J. Fluid Mech.* **186**, 501-520.
- KIRBY, J.T. 1993 A note on Bragg scattering of surface waves by sinusoidal bars. *Phys. Fluids A*, **5**(2), 380-386.
- KIRBY, J.T., DALRYMPLE, R.A. & SEO, S.N. 1987 Propagation of obliquely incident water waves over a trench. Part 2. Currents flowing along the trench. *J. Fluid Mech.* **176**, 95-116.
- LIU, P.L.-F. 1983 Wave-current interactions on a slowly varying topography. *J. Geophys. Res.* **88**(C7), 4421-4426.
- LIU, P.L.-F. 1990 Wave transformation. In B. LeMehaute & D.M. Hanes (eds.) *The Sea*, 9(a), Ocean Eng. Sc., John Wiley, New York.
- LIU, Y. & YUE, D.K.P. 1998 On generalized Bragg scattering of surface waves by bottom ripples. *J. Fluid Mech.*, **356**, 297-326.
- MASSEL, S. R. 1993 Extended refraction-diffraction equation for surface waves. *Coastal Eng.*, **19**, 97-126.
- MILES, J.W. & CHAMBERLAIN, P.G. 1998 Topographical scattering of gravity waves. *J. Fluid Mech.* **361**, 175-188.
- MC KEE, W.D. 1987 Waver waves propagation across a shearing current, *Wave Motion*, Vol 9, 209-215.
- MC KEE, W.D. 1996. A model for surface wave propagation across a shearing current. *J. of Phys. Ocean.* **26**, 276-278.
- MC KEE, W.D. 2003 The propagation of water waves across a shearing current. Rep. Dept of Appl. Math., Univ. of New South Wales AMR 03/26.
- MEI, C.C. 1983 *The applied dynamics of ocean surface waves*. John Wiley & Sons (2nd Reprint, 1994, World Scientific).
- MEI, C.C. 1985 Resonant reflection of surface water waves by periodic sand-bars. *J. Fluid Mech.* **152**, 315-335.

K.A. Belibassakis: Coupled-mode model for water wave scattering by shearing currents in variable bathymetry

- MEI, C.C., HARA, T. & NACIRI, M. 1988 Note on Bragg scattering of water waves by parallel bars on the seabed. *J. Fluid Mech.* **186**, 147-162.
- O'HARE, T.J. & DAVIES, A.G. 1993 A comparison of two models for surface-wave propagation over rapidly varying topography. *Applied Ocean Res.* **15**, 1-11.
- PEREGRINE, D.H. 1976 Interaction of waves and currents. *Adv. Appl. Mech.* **16**, 9-17.
- RECTORYS, K. 1977 *Variational Methods in Mathematics Science and Engineering*, D. Reidel.
- SMITH, J. 1983 On surface gravity waves crossing weak current jets. *J. of Fluid Mech.* **134**, 277-299.
- SMITH, J. 1987 On surface waves crossing a step with horizontal shear. *J. of Fluid Mech.* **175**, 395-412.
- SMITH, J. 2001 Observations and theories of Langmuir circulation: a story of mixing. In J.L. Lumney (eds.) *Fluid Mechanics and the Environment: Dynamical Approaches*, Springer, New York.
- THOMAS, G.P. & KLOPMAN, G. 1997 Wave-current interaction in the nearshore region. In J.N. Hunt (ed.) *Gravity Waves in water of Finite Depth* (Ch. 7), Computational Mechanics Publications.

Appendix A. First variation of the functional \mathcal{F}

In order to derive the first variation of the functional \mathcal{F} defined by Eq. (3.1), we first decompose it into the following terms:

$$\mathcal{F} = \mathcal{F}_a(p) + \mathcal{F}_b(p) + \mathcal{F}_c(p) + \mathcal{F}_d(A_R) + \mathcal{F}_L(p, A_R, \{C_n^{(1)}\}_{n \in N}) + \mathcal{F}_R(p, A_T, \{C_n^{(3)}\}_{n \in N}), \quad (\text{A1})$$

where p stands for $p^{(2)}(x, z)$ in $D^{(2)}$. The various components of \mathcal{F} are defined as follows:

$$\begin{aligned} \mathcal{F}_a &= \frac{1}{2} \int_{D^{(2)}} \left(\left(\nabla \left(\frac{p}{\sigma} \right) \right)^2 + \left(q^2 + \sigma \frac{\partial^2 \sigma^{-1}}{\partial x^2} \right) \left(\frac{p}{\sigma} \right)^2 \right) dx dz, \\ \mathcal{F}_b &= -\frac{1}{2} \int_{\partial D_F^{(2)}} \mu \frac{p^2}{\sigma^2} dS, \quad \mathcal{F}_c = -\frac{1}{2} \int_{\partial D_B^{(2)}} \left(\sigma \frac{\partial}{\partial n} \left(\frac{1}{\sigma} \right) \right) \frac{p^2}{\sigma^2} dS, \quad \mathcal{F}_d = -A_0 A_R J^{(1)}, \quad \text{and} \\ \mathcal{F}_L &= +\frac{1}{\sigma_a^2} \int_{\partial D_i^{(12)}} \left(p - \frac{1}{2} p^{(1)} \right) \frac{\partial p^{(1)}}{\partial x} dS, \quad \mathcal{F}_R = -\frac{1}{\sigma_b^2} \int_{\partial D_i^{(23)}} \left(p - \frac{1}{2} p^{(3)} \right) \frac{\partial p^{(3)}}{\partial x} dS, \end{aligned}$$

where $\sigma_a = \sigma(x=a)$ and $\sigma_b = \sigma(x=b)$. In accordance with the above decomposition, the variation $\delta \mathcal{F}$ of the functional \mathcal{F} is obtained as the sum of the variations of all its components. The variation $\delta \mathcal{F}_a$ is easily calculated to be:

$$\begin{aligned} \delta \mathcal{F}_a &= \int_{D^{(2)}} \left\{ \left(\nabla \frac{p}{\sigma} \right) \nabla \frac{\delta p}{\sigma} + \left(q^2 + \sigma \frac{\partial^2 \sigma^{-1}}{\partial x^2} \right) \frac{p}{\sigma} \right\} \frac{\delta p}{\sigma} dx dz = \\ &= \int_{D^{(2)}} \left\{ -\nabla^2 \frac{p}{\sigma} + \left(q^2 + \sigma \frac{\partial^2 \sigma^{-1}}{\partial x^2} \right) \frac{p}{\sigma} \right\} \frac{\delta p}{\sigma} dx dz + \int_{\partial D_F^{(2)}} \frac{\partial}{\partial n} \left(\frac{p}{\sigma} \right) \frac{\delta p}{\sigma} dS + \\ &+ \int_{\partial D_B^{(2)}} \frac{\partial}{\partial n} \left(\frac{p}{\sigma} \right) \frac{\delta p}{\sigma} dS + \int_{\partial D_i^{(12)}} \frac{\partial}{\partial n} \left(\frac{p}{\sigma} \right) \frac{\delta p}{\sigma} dS + \int_{\partial D_i^{(23)}} \frac{\partial}{\partial n} \left(\frac{p}{\sigma} \right) \frac{\delta p}{\sigma} dS, \quad (\text{A.2}) \end{aligned}$$

where Green's theorem has been applied to functions $\frac{p}{\sigma}$ and $\frac{\delta p}{\sigma}$ in $D^{(2)}$. The variations of the second, third and fourth components, are easily calculated as follows,

$$\delta \mathcal{F}_b = - \int_{\partial D_F^{(2)}} \frac{\mu}{\sigma^2} p \delta p dS, \quad \delta \mathcal{F}_c = - \int_{\partial D_B^{(2)}} \left(\sigma \frac{\partial}{\partial n} \left(\frac{1}{\sigma} \right) \right) \frac{p}{\sigma^2} \delta p dS, \quad \delta \mathcal{F}_d = -A_0 J^{(1)} \delta A_R. \quad (\text{A.3})$$

Gathering all the above four terms, and using $\frac{\partial^2}{\partial x^2} \left(\frac{p}{\sigma} \right) = \frac{1}{\sigma} \frac{\partial^2 p}{\partial x^2} + 2 \frac{\partial \sigma^{-1}}{\partial x} \frac{\partial p}{\partial x} + p \frac{\partial^2 \sigma^{-1}}{\partial x^2}$

and $\frac{\partial \sigma^{-1}}{\partial x} = \frac{q}{\sigma} \frac{\partial U}{\partial x}$, we finally obtain

$$\begin{aligned} \delta (\mathcal{F}_a + \mathcal{F}_b + \mathcal{F}_c + \mathcal{F}_d) &= - \int_{D^{(2)}} \frac{1}{\sigma^2} \left(\nabla^2 p - q^2 p + \frac{2q}{\sigma} \frac{\partial U}{\partial x} \frac{\partial p}{\partial x} \right) \delta p dx dz + \int_{\partial D_F^{(2)}} \frac{1}{\sigma^2} \left(\frac{\partial p}{\partial z} - \mu p \right) \delta p dS + \\ &+ \int_{\partial D_B^{(2)}} \frac{1}{\sigma^2} \frac{\partial p}{\partial n} \delta p dS - A_0 \delta A_R J^{(1)} - \frac{1}{\sigma_a^2} \int_{\partial D_i^{(12)}} \frac{\partial p}{\partial x} \delta p dS + \frac{1}{\sigma_b^2} \int_{\partial D_i^{(23)}} \frac{\partial p}{\partial x} \delta p dS. \quad (\text{A.4}) \end{aligned}$$

For the last two terms in the right-hand side of the above equation use was also made of the fact that both $U(x)$ and $h(x)$ have been assumed to be smooth functions, attaining constant (but possibly different) values at the ends $x=a$ and $x=b$ of the variable bathymetry region, and thus, $\partial\sigma/\partial n=0$ on $\partial D_I^{(12)}$ and $\partial D_I^{(23)}$. Furthermore, using the the outward normal derivative at the bottom $\partial D_B^{(2)}$

$$\frac{\partial p}{\partial n} = - \left(1 + \left(\frac{dh}{dx} \right)^2 \right)^{-1/2} \left(\frac{\partial p}{\partial z} + \frac{dh}{dx} \frac{\partial p}{\partial x} \right), \quad z = -h(x), \quad (\text{A.5})$$

in conjunction with the expression of the surface differential at the bottom $\partial D_B^{(2)}$

$$dS = \sqrt{1 + \left(\frac{dh}{dx} \right)^2} dx, \quad \text{Eq. (A4) takes the form:}$$

$$\begin{aligned} \delta(\mathcal{F}_a + \mathcal{F}_b + \mathcal{F}_c + \mathcal{F}_d) = & - \int_{D^{(2)}} \frac{1}{\sigma^2} \left(\nabla^2 p - q^2 p + \frac{2q}{\sigma} \frac{\partial U}{\partial x} \frac{\partial p}{\partial x} \right) \delta p dx dz + \int_{x=a}^{x=b} \frac{1}{\sigma^2} \left(\frac{\partial p}{\partial z} - \mu p \right) \delta p dx + \\ & - \int_{x=a}^{x=b} \frac{1}{\sigma^2} \left(\frac{\partial p}{\partial z} + \frac{dh}{dx} \frac{\partial p}{\partial x} \right) \delta p dx - A_0 J^{(1)} \delta A_R - \frac{1}{\sigma_a^2} \int_{z=-h_1}^{z=0} \frac{\partial p}{\partial x} \delta p dz + \frac{1}{\sigma_b^2} \int_{z=-h_1}^{z=0} \frac{\partial p}{\partial x} \delta p dS. \quad (\text{A.6}) \end{aligned}$$

We now proceed to calculate the variation of the last two components \mathcal{F}_L and \mathcal{F}_R of the functional, defined on the vertical interfaces $\partial D_I^{(12)}$ and $\partial D_I^{(23)}$ separating the variable depth subdomain $D^{(2)}$ from the left $D^{(1)}$ and the right half strip $D^{(3)}$, respectively. We first consider two harmonic functions Φ, Ψ , defined in the left half-strip and satisfying the modified Helmholtz equation, the linearised free-surface boundary condition and the no-entrance bottom boundary condition. In addition, we suppose the following behaviour of the functions Φ, Ψ at infinity, $x \rightarrow -\infty$

$$\Phi(x, z) = P_0 f(x, z) + P_R f^*(x, z), \quad \Psi(x, z) = p_0 f(x, z) + p_R f^*(x, z), \quad (\text{A.7})$$

where P_0, P_R, p_0, p_R are complex constants, $f(x, z)$ is any bounded function with bounded derivatives and an asterisk symbolizes the complex conjugate. Under condition (A.7), the following relation holds for the Green's integral of these potentials on the vertical boundary $\partial D_I^{(12)}$:

$$\int_{\partial D_I^{(12)}} \left(\Phi \frac{\partial \Psi}{\partial n} - \Psi \frac{\partial \Phi}{\partial n} \right) dS = (-P_0 p_R + p_0 P_R) \cdot J^{(1)}, \quad (\text{A.8a})$$

where $J^{(1)}$ is given by

$$J^{(1)} = 2i \operatorname{Im} \left\{ \int_{z=-h_1}^{z=0} f \frac{df^*}{dx} dz \right\}. \quad (\text{A.8b})$$

Eq. (A.8) is obtained by applying Green's theorem to Φ, Ψ in the left half-strip $D^{(1)}$, taking into account the free-surface and the bottom boundary condition and the asymptotic behaviour of the functions Φ, Ψ at $x = -\infty$. In particular, when $f(x, z) = \exp(ik_0^{(1)}x) Z_0^{(1)}(z)$ and $Z_0^{(1)}(z) = \cosh(k_0^{(1)}(z+h_1))/\cosh(k_0^{(1)}h_1)$, the term

$J^{(1)}$ becomes $J^{(1)} = 2k_0^{(1)} \int_{z=-h_1}^{z=0} \left(Z_0^{(1)}(z) \right)^2 dz$. A similar result can also be established for the harmonic functions Φ, Ψ defined in the right half-strip $D^{(3)}$.

On the basis of Eq. (A.8), we now proceed to calculate the variations $\delta\mathcal{F}_L$ and $\delta\mathcal{F}_R$. The variation $\delta\mathcal{F}_L$ is calculated as follows,

$$\begin{aligned} \sigma_a^2 \delta\mathcal{F}_L &= \delta \int_{\partial D_I^{(12)}} \left(p - \frac{1}{2} p^{(1)} \right) \frac{\partial p^{(1)}}{\partial n^{(1)}} dS = \\ &= \int_{\partial D_I^{(12)}} \delta p \frac{\partial p^{(1)}}{\partial n^{(1)}} dS + \int_{\partial D_I^{(12)}} p \frac{\partial (\delta p^{(1)})}{\partial n^{(1)}} dS - \frac{1}{2} \int_{\partial D_I^{(12)}} \delta p^{(1)} \frac{\partial p^{(1)}}{\partial n^{(1)}} dS - \frac{1}{2} \int_{\partial D_I^{(12)}} p^{(1)} \frac{\partial (\delta p^{(1)})}{\partial n^{(1)}} dS, \end{aligned} \quad (\text{A.9})$$

where $n^{(1)}$ denotes the outward normal vector on the (vertical) boundary $\partial D_I^{(12)}$ of $D^{(1)}$, and thus, $\partial / \partial n^{(1)} = \partial / \partial x$. Taking into account the asymptotic behaviour of the function $p^{(1)}$ in $D^{(1)}$ (given by Eq. 2.10a), for $x \rightarrow -\infty$, and by applying Eqs. (A.8) to the functions $\delta p^{(1)}$ and $p^{(1)}$ on $\partial D_I^{(12)}$, the third term in the right-hand side of Eq. (A.9) is transformed as follows

$$\int_{\partial D_I^{(12)}} \delta p^{(1)} \frac{\partial p^{(1)}}{\partial n^{(1)}} dS = \int_{\partial D_I^{(12)}} p^{(1)} \frac{\partial (\delta p^{(1)})}{\partial n^{(1)}} + A_0 \delta A_R J^{(1)}.$$

Consequently, the variation $\delta\mathcal{F}_L$ is given by the following relation

$$\begin{aligned} \sigma_a^2 \delta\mathcal{F}_L &= \int_{\partial D_I^{(12)}} \delta p \frac{\partial p^{(1)}}{\partial n^{(1)}} dS + \int_{\partial D_I^{(12)}} \left(p - p^{(1)} \right) \frac{\partial (\delta p^{(1)})}{\partial n^{(1)}} dS + A_0 J^{(1)} \delta A_R = \\ &= \int_{z=-h_1}^{z=0} \frac{\partial p^{(1)}}{\partial x} \delta p dz + \int_{z=-h_1}^{z=0} \left(p - p^{(1)} \right) \frac{\partial (\delta p^{(1)})}{\partial x} dz + A_0 J^{(1)} \delta A_R. \end{aligned} \quad (\text{A.10})$$

Similarly, the variation $\delta\mathcal{F}_R$, is calculated as follows:

$$\sigma_b^2 \delta\mathcal{F}_R = \int_{\partial D_I^{(23)}} \delta p \frac{\partial p^{(3)}}{\partial n^{(3)}} dS + \int_{\partial D_I^{(23)}} p \frac{\partial (\delta p^{(3)})}{\partial n^{(1)}} dS - \frac{1}{2} \int_{\partial D_I^{(23)}} \delta p^{(3)} \frac{\partial p^{(3)}}{\partial n^{(3)}} dS - \frac{1}{2} \int_{\partial D_I^{(23)}} p^{(3)} \frac{\partial (\delta p^{(3)})}{\partial n^{(3)}} dS,$$

where $n^{(3)}$ denotes the outward normal vector of the (vertical) boundary $\partial D_I^{(23)}$ of $D^{(1)}$, and thus, $\partial / \partial n^{(3)} = -\partial / \partial x$. By following the same procedure as before, we finally obtain in this case

$$\sigma_b^2 \delta\mathcal{F}_R = - \int_{z=-h_3}^{z=0} \delta p \frac{\partial p^{(3)}}{\partial x} dz - \int_{z=-h_3}^{z=0} \left(p - p^{(3)} \right) \frac{\partial (\delta p^{(3)})}{\partial x} dz. \quad (\text{A.11})$$

Finally, by combining the partial results given by Eqs. (A.6), (A.10) and (A.11), the variation of the functional \mathcal{F} is finally obtained, in the form given by the left-hand side of Eq. (3.3).